PART B:

REACTIVITY METER ANALYSIS OF ROD-DROP EXPERIMENTS IN ZED-2

by

M. Moniz

PART B: McMASTER INDUSTRIAL PROJECT

A project* report submitted in partial fulfillment of the requirements for the degree of
Master of Engineering

Department of Engineering Physics
McMaster University
Hamilton, Ontario

September, 1975

*One of two project reports. The other one is designated PART A: McMASTER (ON-CAMPUS) PROJECT

MASTER OF ENGINEERING
Department of Engineering Physics

MCMASTER UNIVERSITY
Hamilton, Ontario.

TITLE: Reactivity Meter Analysis of Rod-Drop Experiments in Zed-2.

AUTHOR: Manuel S. Moniz, B.Eng. (McMaster)

SUPERVISOR: Dr. R.T. Jones

NUMBER OF PAGES: 56

TABLE OF CONTENTS

LIST OF TABLES

LIST OF TABLES Cont'd

LIST OF FIGURES

LIST OF FIGURES Cont'd

ACKNOWLEDGMENTS

The author wishes to thank the ZED-2 staff, P.D.J. Ferrigan and E.J. Pleau, and D.H. Walker for their assistance during the performance of the experiments. Thanks is also due to P.M. Garvey for his interest and valuable assistance in the theoretical analysis and to G.D. Clark for typing this report.

In particular, the author wishes to extend special thanks and appreciation to R.T. Jones for his supervision and guidance throughout the project.

ABSTRACT

A reactivity meter code based on point kinetics was developed. Rod-drop experiments performed in the ZED-2 reactor tested the code for various detector and rod-drop positions. A delayed neutron hold-up effect was observed whenever a rod was dropped close to a detector. A better understanding of this effect was obtained through a theoretical analysis of the pertinent experiments. The three-dimensional kinetics code, CERBERUS, was used for the theoretical analysis.

1. INTRODUCTION

In recent years the inverse point kinetics technique has gained popularity as a means of providing a fast and viable method for measuring the instantaneous reactivity within a nuclear reactor. Reactivity meters which solve the point kinetics set of equations either by analogue[2] or digital[3,4] means have been described in the literature. Both of these methods have the versatility of being practicable as "on-line" systems which may follow the dynamic behaviour of a multiplying assembly and in so doing become attractive for reactor control.

It is the purpose of this report to investigate the digital approach to the reactivity meter concept through a series of rod-drop experiments performed in the ZED-2 reactor at CRNL. The experiments were designed to test this approach for various flux detector positions with the rod dropped at centre core, and for various rod drop positions with the two detectors at opposite sides of the core. The neutron flux was recorded at consecutive time intervals by two different data handling systems, and then analyzed by a FORTRAN IV computer code which utilized the inverse point kinetics technique to solve for the reactivity versus time.

1.1 Theory

The kinetic behaviour of a reactor may be described by the space-independent point kinetics set of equations:

$$\frac{dN(t)}{dt} = \frac{\rho(t) - \beta}{\ell} N(t) + \sum_{i=1}^{I} \lambda_i C_i(t) + Q \qquad (1)$$

$$\frac{dC_i(t)}{dt} = -\lambda_i C_i(t) + \frac{\beta_i}{\ell} N(t) \qquad (2)$$

where
- $N(t)$ = neutron flux at time t
- $\rho(t)$ = $[K(t) - 1]/K(t)$ = reactivity
- $K(t)$ = effective multiplication factor
- ℓ = neutron generation time
- Q = source strength in neutrons/sec.
- $C_i(t)$ = delayed neutron precursor concentration of the i^{th} group
- λ_i = decay constant of the delayed neutron precursor of the i^{th} group
- β_i = effective delayed neutron fraction of the i^{th} group
- I = total number of delayed groups.

In Appendix A, equations (1) and (2) are rearranged into an integro-differential equation which is then solved numerically to obtain $\rho(t)$, the neutron flux being represented by an interpolation polynomial of second order. The derived expression for the reactivity at a particular time interval, M, is

$$\rho_M = \frac{Q\ell}{N_M} + b \frac{\Delta V_M}{N_M} \{1/2(\alpha_M + 1) + a(\alpha_M - 1)\} + \beta - \sum_{i=1}^{I} \rho_{M,i} \qquad (3)$$

the various symbols being defined in Appendix A.

The first term of the above relation is the reactivity contribution due to a constant source. An

approximate calculation to determine the magnitude of this term for the reactor core used in the experiments showed it to be negligible. The second, or slope, term contains the correction due to the time constant, RC, of the measuring system. This term should become most significant during rapid flux changes.

The major contribution to the reactivity in the situations considered here is the quantity $\beta - \sum_i \rho_{M,i}$, the contribution due to the delayed neutrons, including, for a D_2O moderated reactor, nine photoneutron groups. The delayed neutron fraction, β, is then defined by

$$\beta = \sum_{i=1}^{6} \beta_i + \varepsilon \sum_{j=7}^{15} \beta_j \qquad (4)$$

where β_i = delayed neutron fraction in the i^{th} U-235 group

β_j = delayed neutron fraction in the j^{th} photoneutron group

ε = importance of photoneutrons relative to U-235 delayed neutrons.

In this study no separate allowance was made for delayed neutrons from fast fission of U-238. The decay constants and delayed neutron fractions of the delayed neutron groups used are listed on Table I as obtained from Keepin[1] The photoneutron importance, ε, was obtained from the experiments performed by adjusting it until a relatively constant reactivity occurred in the subcritical region following a rod insertion.

2. EXPERIMENT

Two sets of rod-drop experiments were performed in the heavy-water moderated ZED-2 reactor to provide the

flux-time data required to test the reactivity meter codes. The ZED-2 reactor, shown in Fig. 1, consists of a 336 cm diameter, 333 cm high reactor tank with a 60 cm thick graphite side reflector and a 90 cm thick graphite bottom reflector. The core used consisted of 97 fuel rods on a square lattice with a 28.575 cm pitch. Of these, 69 contained 37-element Bruce D_2O-cooled fuel bundles, while the remaining 28, occupying the perimetral lattice points (see Fig. 2), contained 19-element uranium metal fuel bundles.

2.1 Shutoff Rod and Rod-Drop Mechanism

The shutoff rod used for all the experiments in this report was 48.90 cm long and 3.81 cm O.D. The cylindrical cadmium absorber, 45.72 cm long and 0.381 mm thick, was completely enclosed by aluminum. A thin aircraft cable connected the rod to the pulley of an electric motor. The rod was held up by an electro-magnet, and fell due to its own weight whenever the electro-magnet was turned off. Near the end of a drop, the rod was decelerated by centrifugal brakes attached to the motor shaft. When the rod was fully down, its bottom stood 90 cm from the bottom of the calandria, or approximately at the mid-plane of the reactor where the axial flux distribution peaked.

2.2 Detection and Measurement Systems

Two U-235 fission chambers were strapped to fuel rods such that a detector assumed a position at the cell boundary and at the same height as the shutoff rod. Each fission chamber fed a different data handling system. The first system shown schematically in Fig. 3(a) shall

be called the fast detector because of its shorter sampling time interval, τ. The slow detector is that shown in Fig. 3(b).

The current output from the fast detector was amplified through a Keithley 0-10 volt amplifier whose output was then linearly converted by the voltage-to-frequency (V/F) converter to frequencies in the range 0 - 100 KHz. The output of the V/F converter was fed into a 1024-channel multi-scaler and subsequently punched onto paper tape. It should be mentioned that the values obtained from the multi-scaler represent fluxes averaged within the corresponding time bin.

The slow detector's output was analyzed by the components shown on Fig. 3(b). In this system, the H.P. coupler/controller read flux values represented by the voltage indicated on the digital voltmeter (DVM). The voltage recorded was that existing during the second 1/60 of a second of a sampling time interval, the start of which was indicated by a lamp flashing on the DVM, and the end fixed by the controller so as to be after the teletype had finished printing. Therefore, a flux value obtained from this system was essentially an instantaneous value.

The DVM lamp was used to correlate the timing of the two detectors in the following manner. With the slow detector operating, the multi-scaler was started manually at a particular flash of the lamp. Some number of flashes later the shutoff rod was dropped. Assuming any correlation error to be that due to human reaction time (nominally 0.1 seconds) then the time corresponding to the drop may be in error by as much as 0.2 seconds relative to the fast detector.

2.3 Experimental Method

2.3.1 Varying the Detector Positions

The first set of experiments were designed to test the reactivity meter code for changes in reactivity as the detectors were moved symmetrically across the core, the absorbing rod being dropped at core centre. The various detector positions for each of the four experiments are shown in Fig. 2(a).

The procedure for each experiment was as follows. The heavy water was first pumped into the calandria until the reactor was supercritical. The pumping was then stopped and the reactor power was allowed to increase to 5 watts. The reactor remained critical at this power level for 1 - 1 1/4 hours to ensure saturation of most of the photoneutron precursors. Longer saturating times were not possible due to reactor time scheduling. The critical height of the moderator was noted, and the rod subsequently dropped. For the fast detector τ was set to 0.1 seconds to obtain information during the actual drop. The slow detector had τ set to 2.0 seconds and was left running for 50 - 70 minutes to observe any effects due to the longer-lived photoneutron groups.

After this period, the rod was left in the core while the reactor was again made critical at 5 watts by raising the water level. Twenty minutes at this power level was allowed for most of the delayed neutron groups to saturate. The slow detector was left running during this time. The new critical height was noted and the "neutron flux" registered by each detector. The ratio of the two steady-state fluxes (with and without the rod in) for a detector determined the flux depression experienc by it. The change in the moderator critical height was

used to obtain the reactivity worth of the rod from the level coefficient of reactivity as discussed in Section 3.1.

During the operating time of the slow detector the neutron flux decreased by two decades. This necessitated gain changes of the amplifier.

2.3.2 Rod Depth Versus Time

To aid in analyzing the results obtained during the time the rod was moving, it was decided to try to establish the position of the rod as a function of time. This was accomplished in the following manner. A voltage supply was connected across a helical potentiometer connected to the shaft of the electric motor. The voltage output from the potentiometer was fed through the V/F converter and into the multi-scaler set at 0.1 second per channel. The resultant voltage/time curve for the rod-drop is shown in Fig. 4.

Since one could not assume linearity between voltage output and rod position, it became necessary to correlate the two graphically. The shutoff rod assembly was removed from the core and the rod was raised to positions measured on a two-metre scale. The corresponding voltages were obtained from the DVM connected to the helipot. The results obtained are shown in Fig. 5, the non-linearity existing as expected. The two curves were then unfolded and the rod depth versus time curve of Fig. 6 was obtained, the deceleration of the rod near the bottom being quite noticeable.

2.3.3 Varying the Rod-Drop Position

This set of experiments was performed to compare the time-dependant fluxes on opposite sides of the core as

the rod position was varied across one half of the core. The four rod-drop locations and the detector positions are shown on Fig. 2(b). At the start of the first experiment the amplifier of the fast detector failed and was replaced by a Radiation Detection Amplifier (EB-5530) built at CRNL.

The experimental procedure was the same as for the previous experiments except that τ for the fast detector was increased to 0.8 seconds. The operating time of the slow detector was also decreased to 800 - 1000 seconds to roughly match that of the other detector.

3. RESULTS AND ANALYSIS

3.1 Level Coefficient of Reactivity

The reactivity worth of the shutoff rod in each of the experiments was calculated from the change in moderator critical height and the level coefficient of reactivity as outlined in Ref. (5) and (6). The level coefficient of reactivity, (LCR), is defined as LCR = $d\rho/dh$ where h is the moderator height.

The reactivity effect of the shutoff rod may then be obtained from

$$\rho = \int_{h_0}^{h_1} \frac{d\rho(h)}{dh}\, dh$$

where h_0 = unperturbed critical height,
h_1 = critical heigth with rod in.

In the one-group, bare reactor model the level coefficient of reactivity is inversely proportional to the cube of the extrrapolated height. Assuming that the deviation from this relationship is small in a reflected core, it can be shown that[5]

$$\rho = [LCR_0(H_0/H_1) + LCR_1(H_1/H_0)] \left(\frac{h_0 - h_1}{2}\right) \quad (5)$$

where LCR_0 and LCR_1 are the level coefficients at critical heights h_0 and h_1 respectively, and H_0 and H_1 are the extrapolated heights.

From previous measurements of LCR's obtained for this core, a straight line plot of H_{ex}^3 versus LCR (Fig. 7) provided the relation.

$$LCR = -4.3226 \times 10^{-8} H^3 + 1.1901 \quad (6)$$

From this, the level coefficients for the rod in and out of the core were obtained for each experiment and are listed on Table III. The corresponding reactivities were then calculated from equation (5).

The change in reactivity as the detector positions are radially varied (Table II) is due to the changing shadowing effect of the shutoff rod on the detectors.

3.2 The Reactivity Meter Code

From the description of the experimental procedure it is expected that the reactivity calculated by the meter code will be as follows. Zero for the critical reactor followed by a rapid drop to some negative value at the moment of the rod insertion. This negative value should then be maintained constant for all time until some further change is made to the reactor, such as the re-establishment of the critical state, by increasing the critical height, as was recorded by the slow detector.

To obtain constant reactivity from the code after the drop, several photoneutron parameters can be adjusted, namely ε and the W_i's defined in Appendix A. The delayed neutron precursors were all assumed to be fully saturated before the rod drop - i.e. the W_i's were set equal to 1. Thus only ε was varied.

Also the time constant of the instrumentation was assumed to be 1 ms. Table III shows that any substantial error in the reactivity resulting from an incorrect RC value will occur only during the first second of the drop, becoming much less than experimental error after 2 seconds.

3.2.1 Varying the Detector Positions

Figures 8 - 11 show the reactivity/time curves obtained from the meter code for both detector positions in the first four experiments. One interesting feature of these curves is the rise in reactivity, shown in Fig. 8, following a rod-drop one pitch distance from the detectors. This effect is presumably a spatial one, caused by the localized flux depression around the rod. This then illustrates an inadequacy of the point kinetics reactivity meter, namely that care must be taken with detector positioning if a reasonable approximation to the global, or space-independent, neutron flux is to be measure

The expected sharp drop to a constant negative reactivity is well illustrated by the results from the fast detector, particularly in Fig. 9(b). It is also reproduced from the slow detector's output, though not as well since it becomes more difficult to maintain a constant reactivity at long times by solely adjusting ε (e.g. Fig. 11(a)). By then, the longer-lived photoneutron precursors are a major souce of neutrons in the reactor, and so their densities prior to the rod-drop (which were assumed saturated) become important..

The expected rise to a positive reactivity and subsequent drop to zero at criticality are observed in Figures 9(a), 10(a) and 11(a). Figure 10 also shows the flux/time curve obtained from both detectors. The

increased reactivity fluctuations after long times are due to the smaller signal-to-noise ratio at low neutron fluxes. The spurious effects observed during the first 300 - 400 seconds (see Fig. 10(a)) are attributable to the amplifier gain changes previously mentioned.

To try to establish the reactivity worth of the rod as determined by the meter code, the reactivities were averaged over a time span in which they remained relatively constant. These averaged values, together with their corresponding ε values, are shown in Table IV. The errors shown are the standard deviations from the above averaging procedure. A comparison of the reactivities calculated from the moderator level coefficient to those from the meter (also on Table IV) shows reasonable agreement, the largest discrepancy being ~11%.

3.2.2 Varying the Rod-Drop Position

The reactivity-time curves for the last four experiments are shown in Figs. 12-15. The reactivity meter is again failing to produce a well-defined step drop in reactivity to a constant value. It does, however, show the decrease in the reactivity worth of the rod as its position is moved to lower flux regions.

The results from the fast detector show slow variations in the reactivity for ~300 seconds following the drop. This is very noticeable in Figs. 12(b) and 13(b), and could not be removed by varying ε. The amplifier for this detector was replaced in these experiments by one of unknown performance (see Section 2.3.3). The above effects may therefore be due to non-linearities at low output voltages.

The spatial effect observed before is also reproduced in Figs. 14(a) and 15(a) where the rod was dropped near the detector. The prompt-drop to asymptotic reactivity ratio increases from 1.26 to 1.54 as the rod is moved closer to the detector.

As for the previous set of experiments, a reactivity worth of the rod at each position was obtained and is given in Table IV. The agreement between these values and those obtained from the level coefficient is better than 12%, as before.

3.3 Discussion on ε

From Table V one can see that ε varies (in an unsystematic way) by as much as 46%, both between experiments and between detectors. Since ε was the parameter adjusted to maintain constant reactivity in the subcritical region, it may in fact have been changed to cover up other effects. These could include amplifier non-linearties at low output voltages; errors caused by gain changes; errors arising from the assumption that the photoneutron precursors were fully saturated before the rod-drop, or small temperature drifts in the reactor in this time interval.

Overestimating ε will introduce more photoneutrons than are physically present in the reactor, resulting in an increasingly negative reactivity at long times. The reverse is true when ε is underestimated. The results of Fig. 14(b) (ε = 0.4) were reproduced for ε = 0.41, 0.43, 0.45 and 0.47 to determine the respective error variations in time. Assuming ε = 0.4 to be the correct value, the errors in reactivity were then obtained from the relation

$$[\rho(t,\varepsilon) - \rho_0(t)]/\rho_0(t) \qquad (7)$$

where $\rho_0(t)$ is the reactivity for $\varepsilon = 0.4$. Fig. 16 shows this error as a function of time and ε. The time scale is the same as in Fig. 14(b), the rod-drop occuring after 67 seconds. A proportionate decrease in ε resulted in the same error profile but reversed in sing.

Note that for ~100 seconds after the drop the error arising from a 20% change in ε is 3.2%, or less than experimental error, indicating that this region is relatively insensitive to ε.

4. THEORETICAL ANALYSIS

To check on the spatial effects detected by the reactivity meter, a theoretical analysis of the pertinent experiments was undertaken. A two-group three-dimensional kinetics code called CERBERUS was used which is based on the improved quasi-static method of Ref. (7). In this method, the total flux, $\Phi(\bar{r}, E, t)$ is factorized into an amplitude function, $\phi(t)$, and a shape function, $\psi(\bar{r},E,t)$:

$$\Phi(\bar{r},E,t) = \phi(t)\ \psi(\bar{r},E,t);\ \phi(o) = 1.0 \qquad (8)$$

The assumption is made that the time dependence of the shape function is of lesser importance than that of the amplitude function. Therefore, the code calculates many values of the amplitude along the time axis but only a few shape functions. The precursor density distributions are calculated directly from the flux history.

The approximation to the ZED-2 core shown in Fig. 17 was fed into the CERBERUS code. Symmetry was assumed in the y-direction thus cutting the core in half. The core was divided into cells, 28.575 cm square and 27.0 cm high, of three different materials: the two fuel materials and a D_2O reflector. The axial height of the core was taken to be 270 cm, the extrapolated height. The cell parameters

required for CERBERUS for each material type were obtained from the code, LATREP[8]. These and other required parameters are defined in Appendix B.

The shutoff rod length was set equal to the height of the two cells, 54 cm. It was represented as a fourth material with the same properties as the Bruce fuel, except for the thermal group neutron absorption cross-section. The rod-drop was approximated by dividing the time of the drop into six intervals. Each interval represented the time it took the rod to fall a distance equal to a cell height, as determined from Fig. 6. These time intervals and the corresponding axial cell into which the rod fell are given in Table V.

The CERBERUS code was modified to incorporate all 15 delayed neutron groups, and to calculate the reactivity by inverse point kinetics from the flux change at a particular cell. This cell was made to correspond to a detector location for direct comparison between theory and experiment. The detectors were placed in the sixth axial cell in CERBERUS, the X-Y co-ordinates being varied according to experiment.

4.1 Results and Analysis

The first run of CERBERUS was a static case to insure that the correct eigenvalue was calculated and that the flux profiles seemed sensible. For the second run, also a static case, the rod was introduced at O1W (cells (4,8,6) and (4,8,7) in CERBERUS). The thermal absorption cross section was then adjusted until the global reactivity calculated by CERBERUS matched that obtained from the level coefficient for the corresponding experiment. The cross-section finally obtained was $0.00755\ cm^{-1}$.

A full kinetics analysis for a 120 second interval was then obtained from CERBERUS for the rod-drop at O1W. Fig. 18 shows the reactivity calculated from the CERBERUS flux at the two detector positions, O1E (4.7.6) and G1E (12, 7, 6). The third curve is the global reactivity calculated by CERBERUS. The time dependence shown is in good qualitative agreement with experimental results, shown in Fig. 15, for both detectors. Quantative discrepancies are attributable to the oversimplification in modelling the ZED-2 core and the rod-drop.

The spatial effect, observed both experimentally and theoretically, is due to the time delay of the adaptation of the precursor spatial distribution to the perturbed flux shape. When the rod is dropped close to a detector, a localized flux depression occurs. However, the precursor spacial distribution still follows that of the unperturbed flux, decaying asymptotically to the perturbed flux distribution. The reactivity, therefore, will increase to a smaller asymptotic negative value as the original precursor densities continue to decay.

An absorbing rod dropped in one half of the core excites the first azimuthal mode causing a positive flux tilt in the other half. However, the unperturbed precursor density distribution is still decaying. This results in the prompt drop in reactivity being retarded (as shown in Figs. 17 and 22) as the neutron contribution from the original precursor distribution dies away with time. This delayed neutron hold-up effect is not as pronounced as in position O1E where a greater change in the flux distribution occurs.

The delayed neutron hold-up also effects the global reactivity calculated by CERBERUS. This is more important in large, loosely coupled reactors where big flux tilts can develop, but is hardly noticeable in ZED-2.

The next CERBERUS run analyzed the rod-drop at position N1W. The resultant reactivity versus time curves are shown in Fig. 19. Again the temporal distribution is in good qualitative agreement with the experimental results shown in Fig. 14. The precursor hold-up effect is clearly reproduced at both detector positions.

The rod-drop at centre core, the detectors being located at L1E and J1E, was also analyzed by CERBERUS. Fig. 20 shows that CERBERUS calculated identical reactivities at both detector positions due to the symmetry in the X-direction. The results are in good agreement with the experimental results shown in Fig. 8.

Figs. 8(a) and 20 show a rise in reactivity during the first 200 seconds. However, the reactivity obtained from the fast detector results (Fig. 8(b)) was made constant during this time interval by varying ε. From Table IV one can see that this ε was overestimated when compared to that obtained from the slow detector results. Thus it now seems incorrect to have adjusted ε over this short time interval where significant effects from the delayed neutron precursor hold-up may occur.

5. FAST TRANSIENT ANALYSIS

The fast detector was originally run with $\tau = 0.1$ seconds to obtain information on fast transients during the drop. The experiment considered for this analysis was that in which the detector was located at G1E and the rod at centre core (Fig. 11(b)). The flux/time profile obtained from the detector plus the meter code analysis of the drop are shown in Fig. 21. The results from the meter code are also shown with those of the rod depth versus time curve in Fig. 6.

The slope term mentioned in Section 1.1 should become significant in this analysis, the fastest flux changes occuring during the drop. However, the meter code's results showed that at its maximum the slope term contributed only 0.16 mk or ~25% of the total reactivity. Furthermore, this contribution quickly decreased to less than 2% after only 5 seconds from the initiation of the rod-drop.

5.1 Comparison with CERBERUS

The kinetics code, CERBERUS, was also used to analyze the above experiment. Its results are compared in Fig. 21 with those obtained from the meter code. The agreement between the two indicates that the rod-drop was well approximated in CERBERUS. The discrepancy near the end of the fall could perhaps be removed by obtaining more axial rod positions during this interval, thus providing a better rod-drop approximation.

6. SUMMARY

The main objective of the rod-drop experiments performed was to test the feasibility of a reactivity meter code based on the point kinetics model. It has been shown that the meter code reproduces reasonably well the expected step drop in reactivity due to a rod insertion and subsequent changes when the moderator level is again increased. However, there are some limitations. The inability of a single detector to measure a global neutron flux results in spatial effects attributed to delayed neutron hold-up. For analysis over long times, the photoneutron parameters become very important, ε in particular, unless one is interested only in the prompt reactivity drop.

Consideration should be given to further testing of the code, concentrating on the problems disclosed by this project. For example, the problem of obtaining a global neutron flux may be minimized by positioning the detector at a predetermined location in the core where the local flux perturbation is expected to be minimal. Or the outputs of two or more detectors may be summed as one in anticipation that spatial errors may cancel and a better approximation to the true global flux is obtained. More long-term experiments utilizing an autoranging amplifier should be performed to remove errors due to scale changes and to gain information and experience on the proper adjustment of the photoneutron parameters.

APPENDIX A

DERIVATION OF THE INVERSE NEUTRON KINETICS EQUATIONS

Equations (1) and (2) in the text may be expressed as an intergo-differential equation:

$$\rho(t)\, N(t) = \ell\, [\frac{dN(t)}{dt} - Q] + \beta N(t) - \sum_i \beta_i \lambda_i \int_{-\infty}^{t} N(t') e^{\lambda_i (t'-t)}\, dt'$$

Experimentally, the neutron flux, N, is averaged over a sampling time interval, τ, such that at the M^{th} time interval

$$N_M = 1/\tau \int_{(M-1)\tau}^{\tau} N(t')\, dt'$$

The flux within a time interval may be approximated by a second degree interpolation polynomial of the form

$$N_M(t) = a_{0M} + a_{1M} t + a_{2M} t^2$$

where

$$a_{0M} = N_M - \Delta N_M [1/2\, M^2 (1 - \alpha_M) + M\alpha_M - 1/6\, (1 + 2\alpha_M)]$$

$$a_{1M} = (\Delta N_M/\tau)\, [M(1 - \alpha_M) + \alpha_M]$$

$$a_{2M} = (1/2\, \Delta N_M/\tau^2)\, (\alpha_M - 1)$$

$$\Delta N_M = N_M - N_{M-1}$$

$$\alpha_M = \frac{\Delta N_{M+1}}{\Delta N_M}$$

In reality the flux values will be voltages measured by some electronic circuity, like that of Fig. 3. For fast changes in flux (such as shut down) the time constant of the instrumentation may become important. Thus the flux may then be represented in terms of the voltage, V(t), by

$$N(t) = V(t) + RC\, dV(t)/dt \tag{4}$$

where V(t) is approximated by the interpolation polynomial of equation (3).

Using the neutron flux weighted mean reactivity defined in Ref. 4, the reactivity at the M^{th} time interval becomes

$$\rho_M = \left[\int_t^{t+\tau} \rho(t')N(t')dt'\right] \Big/ \left[\int_t^{t+\tau} N(t')dt'\right]$$

$$= \left[\int_t^{t+\tau} \rho(t')N(t')\, dt'\right] \Big/ N_M\tau \tag{5}$$

Substituting the above into equation (1) and rearranging terms one obtains

$$\rho_M = \frac{\ell}{N_M\tau} \int_{(M-1)\tau}^{M\tau} \left[\frac{dN(t')}{dt'} - Q\right]dt' + \beta - \sum \frac{\beta_i\lambda_i}{iN_M\tau} \int_{(M-1)\tau}^{M\tau} dt'$$

$$\int_{-\infty}^{t} N(t'')e^{-\lambda_i(t''-t'')}\, dt'' \tag{6}$$

Integrating the first term of the above expression and then substituting equation (3) and (4) into the result yields

$$\frac{\ell}{N_M} \{\Delta V_M[1/2\,(\alpha_M + 1) + a(\alpha_M - 1)] - Q\tau\} \tag{7}$$

where $a = RC/\tau$.

Further subdivision produces two terms already defined as the slope term:

$$b\,\frac{\Delta V_M}{N_M}\,[1/2(\alpha_M + 1) + a(\alpha_M - 1), \quad b = \ell/\tau \tag{8}$$

and the source term: $Q\ell/N_M$ (9)

The last term in equation (6), after simple but tedious manipulations, reduces to a recursion formula for each percursor group, i, of the form

$$\rho_{M,i} = \frac{1}{N_M}\left[N_{M-1}\, e^{-\lambda_i \tau}\, \rho_{M-1,i} + R_{M,i}\right] \tag{10}$$

where $R_{Mi} = V_M A_{o_i} + \Delta V_M \left[B_2 + \alpha_M B_{1i} + a\,(C_{oi} + \alpha_M C_{1i})\right]$

$$A_{oi} = \beta_i\left[1 - e^{-\lambda_i \tau}\right]$$

$$B_{oi} = \beta_i\left[e^{-\lambda_i \tau}\left(1 + \frac{3}{2\lambda_i \tau} + \frac{1}{\lambda_i^2 \tau^2}\right) - \frac{1}{2\lambda_i \tau} - \frac{1}{\lambda_i^2 \tau^2}\right]$$

$$B_{1i} = \beta_i\left[\frac{1}{\lambda_i^2 \tau^2} - \frac{1}{2\lambda_i \tau} - e^{-\lambda_i \tau}\left(\frac{1}{2\lambda_i \tau} + \frac{1}{\lambda_i^2 \tau^2}\right)\right]$$

$$C_{oi} = \beta_i\left[\frac{1}{2} + \frac{1}{\lambda_i \tau} - e^{-\lambda_i \tau}\left(\frac{3}{2} + \frac{1}{\lambda_i \tau}\right)\right]$$

$$C_{1i} = \beta_i\left[\frac{1}{2} - \frac{1}{\lambda_i \tau} + e^{-\lambda_i \tau}\left(1/2 + 1/\lambda_i \tau\right)\right]$$

These equations differ somewhat from those of Ref. 4. However, it was found that the results from Ref. 4 do not work satisfactorily as is easily seen by solving the equations derived in this reference for the constant flux case. The resultant reactivity should be zero, but is not. Equation (10), meanwhile, does yield zero reactivity for the same case.

For the initial time interval equation (6) was re-solved to obtain a new recursion formula.

$$\rho_{1,i} = 1/N_1\left[V_a W_i/\lambda_i \tau\; A'_{o,i} + R'_{1,i}\right] \tag{11}$$

where $R'_{1,i} = U_1 A'_{oi} + \Delta V_i\left[B'_{o,i} + \alpha_1 B'_{1,i} + a(C'_{o,i} + \alpha_1 C'_{1,i})\right]$

$$A'_{o,i} = C[\lambda_i\tau + e^{-\lambda_i\tau} - 1]$$

$$B'_{o,i} = C[1/\lambda_i{}^2\tau^2 - 1/6 - e^{-\lambda_i\tau}(1/3 + 1/\lambda_i\tau + 1/\lambda_i{}^2\tau^2)]$$

$$B'_{1,i} = C[1/\lambda_i\tau - 1/3 - 1/\lambda_i{}^2\tau^2 + e^{-\lambda_i\tau}(1/\lambda_i{}^2\tau^2 - 1/6)]$$

$$C'_{o,i} = C[\lambda_i\tau/2 - 1/\lambda_i\tau + e^{-\lambda_i\tau}(1 + 1/\lambda_i\tau)]$$

$$C'_{1,i} = C[\lambda_i\tau/2 - 1 + 1/\lambda_i\tau - e^{-\lambda_i\tau}(1/\lambda_i\tau)]$$

$$c = \beta_i/(\lambda_i\tau)$$

$$W_i = \lambda_i/V_a \int_{-\infty}^{o} e^{\lambda_i t'} N(t')\, dt'$$

V_a = initial neutron flux.

Thus the reactivity at a particular time interval, M, is obtained from the expression

$$\rho_M = Q\ell/N_M + b\ \Delta V_M/N_M \{1/2(\alpha_M + 1) + a(\alpha_M - 1)\}\beta + - \sum_i \rho M_i -$$

(12)

APPENDIX B

INPUT PARAMETERS FOR CERBERUS

The following are the material properties, neutron velocities and the convergence criteria as required by CERBERUS. The spatial parameters and materials distributions are covered in the text.

PROPERTY	MATERIAL TYPE		
	1	2	3
GROUP 1 Diffusion	1.212	1.2297	1.3538
GROUP 2 Diffusion	0.9897	0.9937	1.1340
GROUP 1 Absorption	0.0	0.00105	0.0010
GROUP 2 Absorption	9.92×10^{-5}	0.00429	0.00494
FAST PRODUCTION	0.0	0.0056	0.00600
FAST REMOVAL	0.0106	0.00971	0.00932

NEUTRON VELOCITIES: $V_1 = 1.0 \times 10^7$ cm.sec^{-1}

$V_2 = 2.20 \times 10^5$ cm.sec^{-1}

CONVERGENCE CRITERION: 0.001

LIEBMANN ACCELERATION PARAMETER: 1.7

MAXIMUM NUMBER OF ITERATIONS: 1000

REFERENCES

1. KEEPIN, G.R., "Physics of Nuclear Kinetics", Addison-Wesley Publising Co., Inc., (1965).

2. SASTRE, G.A., "The Measurement of Reactivity", Nucl. Sci. & Engin., 8, 443-447 (1960).

3. CARPENTER, S.G., "Reactivity Measurements in the Advanced Epithermal Thorium Reactor Critical Experiments", Nucl. Sci. & Engin., 21, 429, (1965).

4. ANSELMI, L., et al, "Aspects in the Use of the Inverse Neutron Kinetics Technique", Nucl. Inst. & Mech., 98, 485-491 (1972).

5. SRINIVASAN, M., Atomic Energy of Canada Limited Unpublished Report, CRNL-884, (1973).

6. OKAZAKI, A., JONES, R.T., "Additional Shutoff Rod Experiments in ZED-2", Atomic Energy of Canada Limited Report, AECL-5102, (1975).

7. OTT, K.O., MENELEY, D.A., "Accuracy of the Quasistatic Treatment of Spatial Reactor Kinetics", Nucl. Sci. & Engin., 36, 402 - 411, (1969).

8. PHILLIPS, G.J., GRIFFITHS, J. "LATREP User's Manual", CRNL-543, (1971).

TABLE I

DELAYED NEUTRON DATA

U-235 DELAYED GROUPS: -

RELATIVE FRACTION (β_i)	DECAY CONSTANT (s^{-1})
0.033	0.0124
0.219	0.035
0.196	0.111
0.395	0.301
0.115	1.13
0.042	3.0

PHOTONEUTRON DELAYED GROUPS: -

β_p	λ_p (s^{-1})
0.6464	0.277
0.2025	0.0169
0.0695	0.00481
0.0333	0.0015
0.0205	4.28×10^{-4}
0.0231	1.16×10^{-4}
0.0032	4.39×10^{-5}
0.001	3.65×10^{-6}
0.005	1.63×10^{-6}

TABLE II

CRITICAL HEIGHT CHANGES AND REACTIVITIES

SITION OF DETECTOR OR ROD	DATE	ROD STATUS	H_c(cm)	ΔH (cm)	LCR	ρ(mk)
) *VARYING DETECTOR POSITIONS*						
J1E/L1E	May 27 (a.m.)	Out (of core)	247.546		.3496	
		In	257.330	9.784	.2544	2.935
I1E/M1E	May 27 (p.m.)	Out	246.960		.3551	
			257.308	10.348	.2545	3.130
H1E/N1E	May 28 (a.m.)	Out	246.367		.3606	
		In	256.779	10.412	.2600	3.207
G1E/O1E	May 28 (p.m.)	Out	245.613		.3676	
		In	256.000	10.387	.2678	3.276
) *VARYING ROD POSITIONS*						
L1W	May 29 (a.m.)	Out	245.775		.3661	
		In	255.388	19.613	.2739	3.057
M1W	May 29 (p.m.)	Out	245.801		.3658	
		In	253.580	7.779	.2917	2.548
N1W	May 30 (a.m.)	Out	245.830		.3656	
		In	251.314	5.484	.3137	1.859
O1W	May 30 (p.m.)	Out	245.845		.3654	
		In	249.176	3.331	.3342	.164

TABLE III

VARYING THE TIME CONSTANT, RC

TIME (sec)	RC VALUES .01	.0001	.00001
.1	$\frac{\rho(RC)^*}{\rho_o}$ = 1.185	.9816	.9797
.2	1.148	.9852	.9838
.3	1.125	.9875	.9863
.5	1.072	.9928	.9921
.7	1.049	.9951	.9946
.9	1.034	.9965	.9962
1.1	1.023	.9977	.9975
2.1	1.005	.9995	.99945
2.6	1.003	.9997	.99965
3.1	1.002	.9998	.9998
.			
.			
.			
100.0	1.0008	.9993	.99992

* $\rho_o = \rho(RC = .001)$

TABLE IV

REACTIVITIES AS DETERMINED BY THE REACTIVITY METER

OSITION OF TECTORS OR ROD	FAST DETECTOR		SLOW DETECTOR		ρ_{LCR}
	ρ(mk)	ε	ρ(mk)	ε	
a) *VARYING DETECTOR POSITIONS*					
JkE/L1E	3.283 ± .034	0.396	3.033 ± .059	0.305	2.935
I1E/M1E	3.286 ± .023	0.39	3.070 ± .066	0.34	3.130
H1E/N1E	3.149 ± .023	0.28	3.101 ± .053	0.325	3.207
G1E/O1E	3.118 ± .025	0.28	3.037 ± .056	0.40	3.276
b) *VARYING ROD DROP POSITIONS*					
L1W	2.885 ± .032	0.36	2.887 ± .061	0.41	3.057
M1W	2.366 ± .068	0.305	2.521 ± .052	0.40	2.548
N1W	1.652 ± .038	0.33	1.720 ± .041	0.30	1.359
O1W	1.031 ± .018	0.33	1.019 ± .018	0.28	1.164

TABLE V

APPROXIMATING THE ROD-DROP INTO APPROPRIATE TIME INTERVALS FOR CERBERUS

TIME INTERVAL (sec)	AXIAL CELL
0.15	2
0.25	2 and 3
0.40	3 and 4
0.50	4 and 5
0.65	5 and 6
1.30	6 and 7

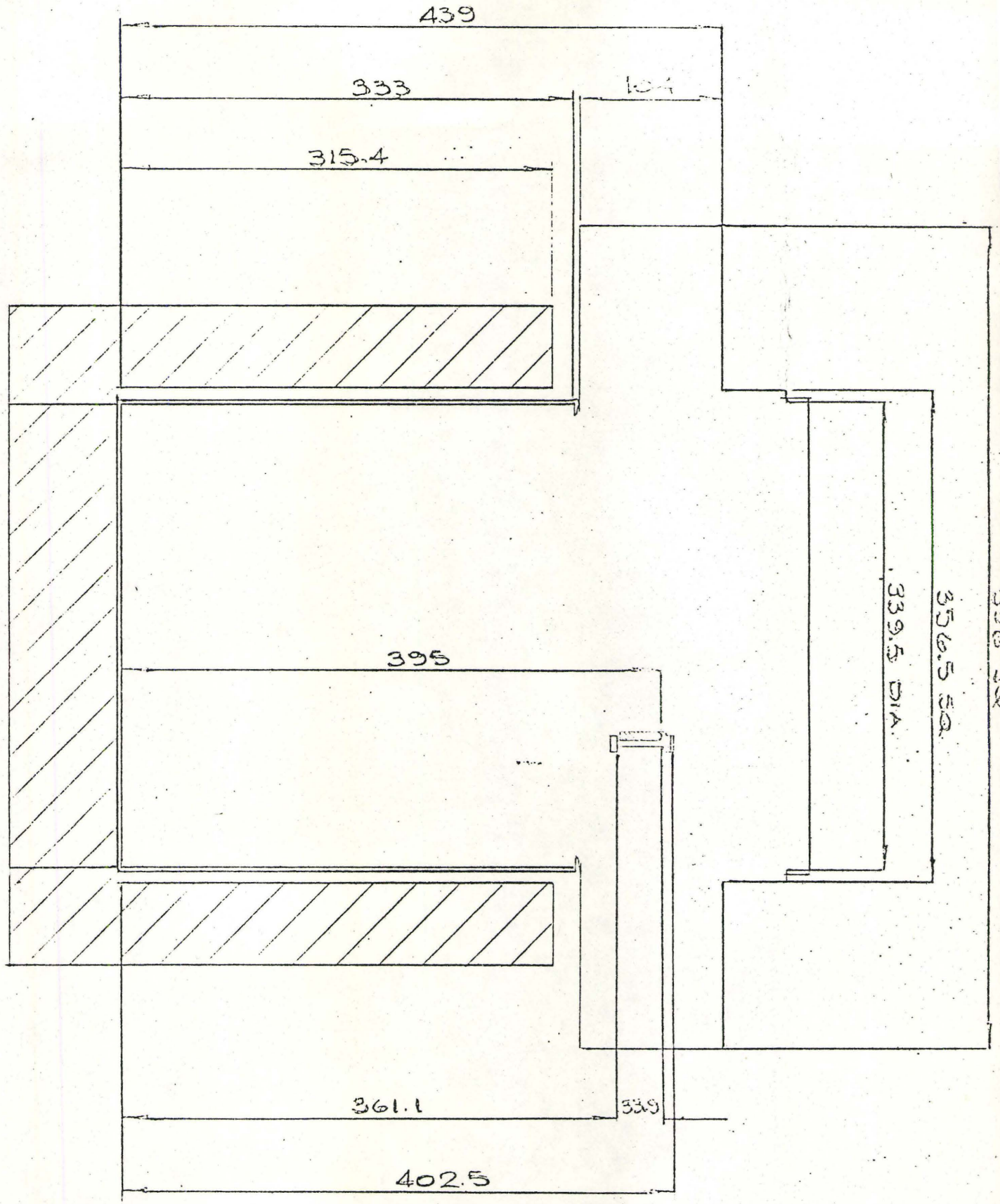

FIG. 1: SCHEMATIC SECTION OF ZED-2

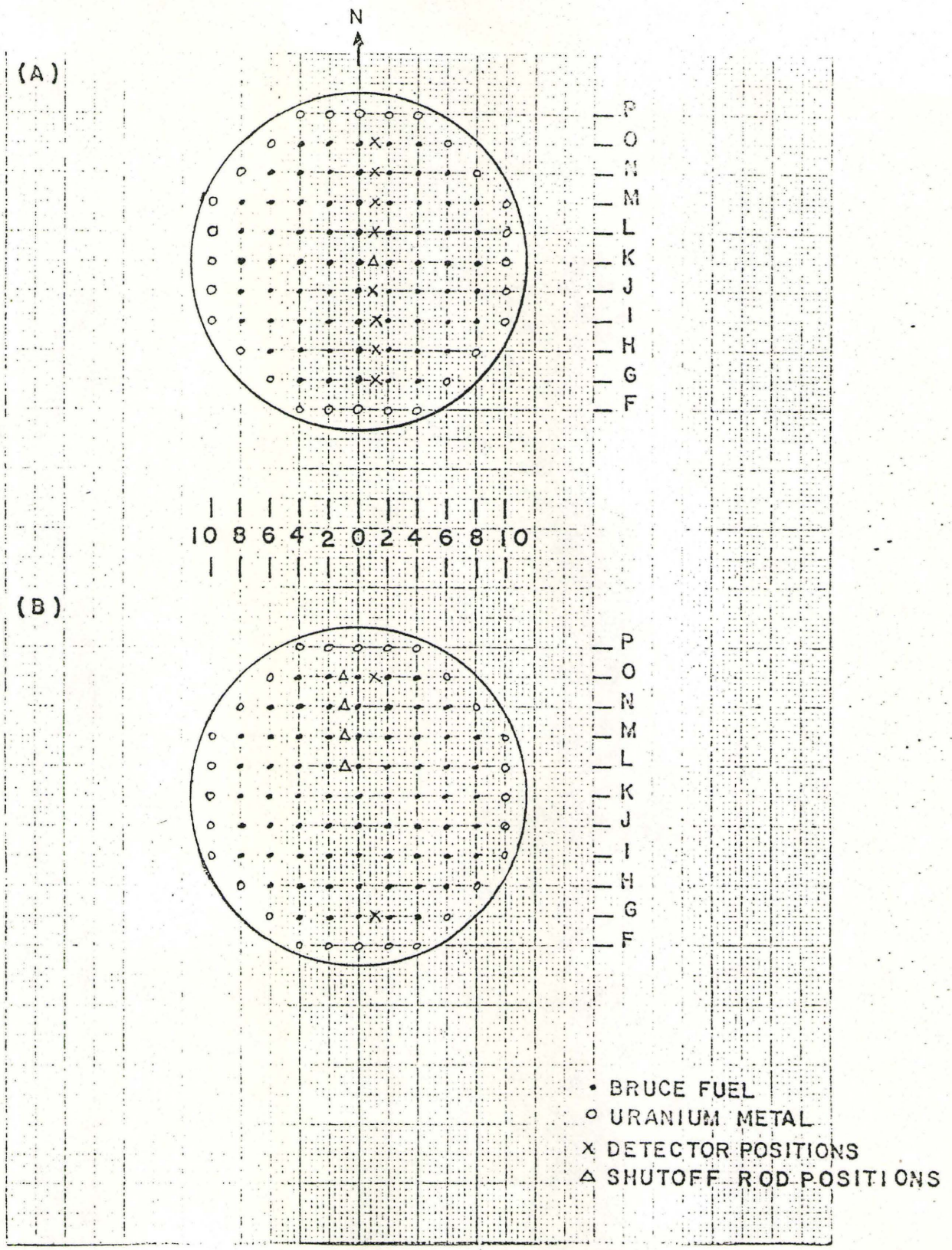

FIG. 2: DETECTOR POSITIONS, (A), AND RCD POSITIONS, (B), FOR THE ROD-DROP EXPERIMENTS

(A)

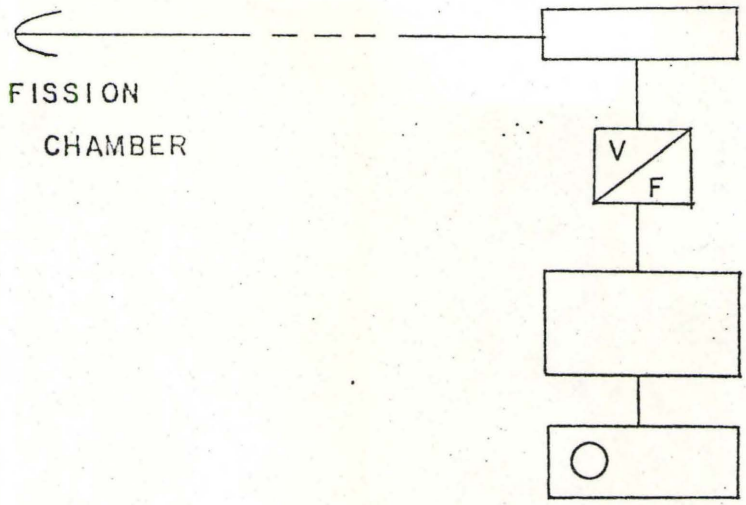

KEITHLEY AMPLIFIER
(0-10 VOLTS)

DATEL VOLTAGE-FREQUENCY
CONVERTER

N.D.C. MULTI-SCALER

TALLY-420 PAPER TAPE
DRIVE

(B)

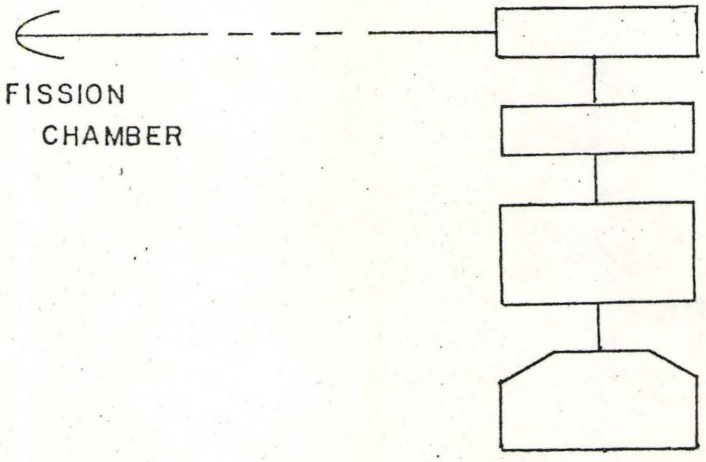

KEITHLEY AMPLIFIER
(0-3 VOLTS)

H.P. 3460A DVM

H.P. 2570A COUPLER-
CONTROLLER

TELETYPE AND PAPER
TAPE PUNCH

FIG. 3: SCHEMATIC OF FAST DETECTOR, (A), AND SLOW DETECTOR (B), SYSTEMS

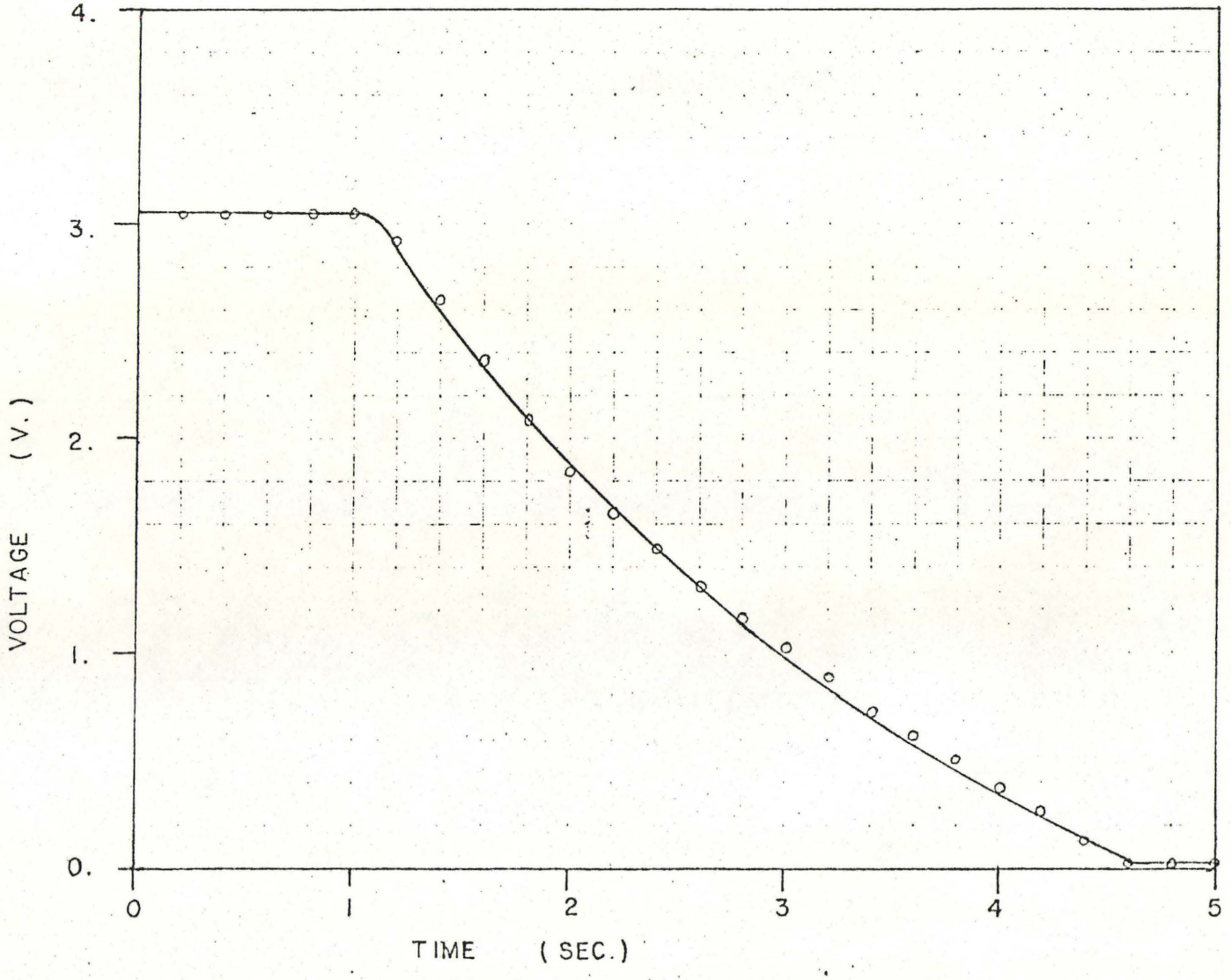

FIG. 4: VOLTAGE VERSUS TIME FOR THE ROD DROP

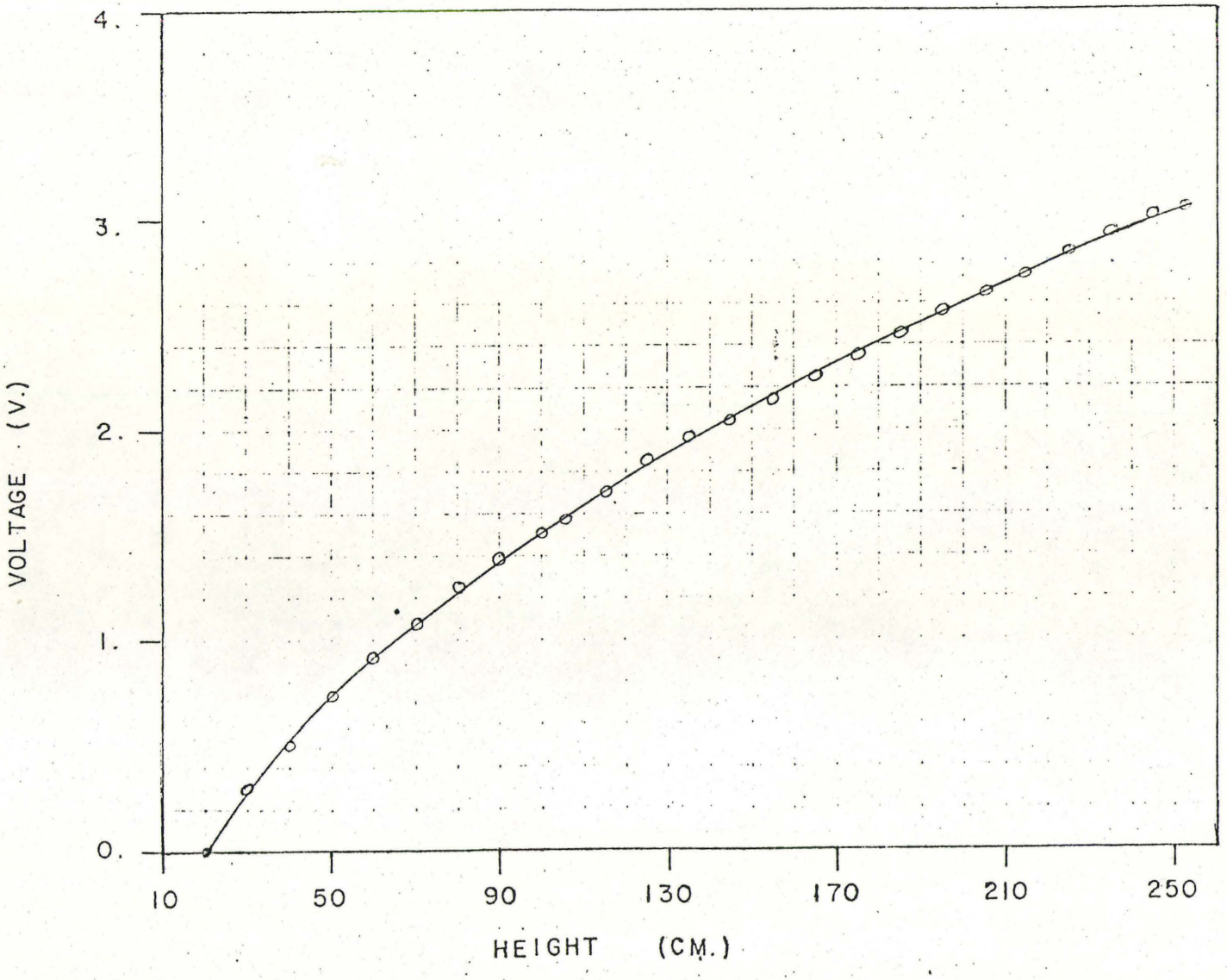

FIG. 5: RELATION BETWEEN VOLTAGE AND ROD POSITION DURING THE ROD DROP

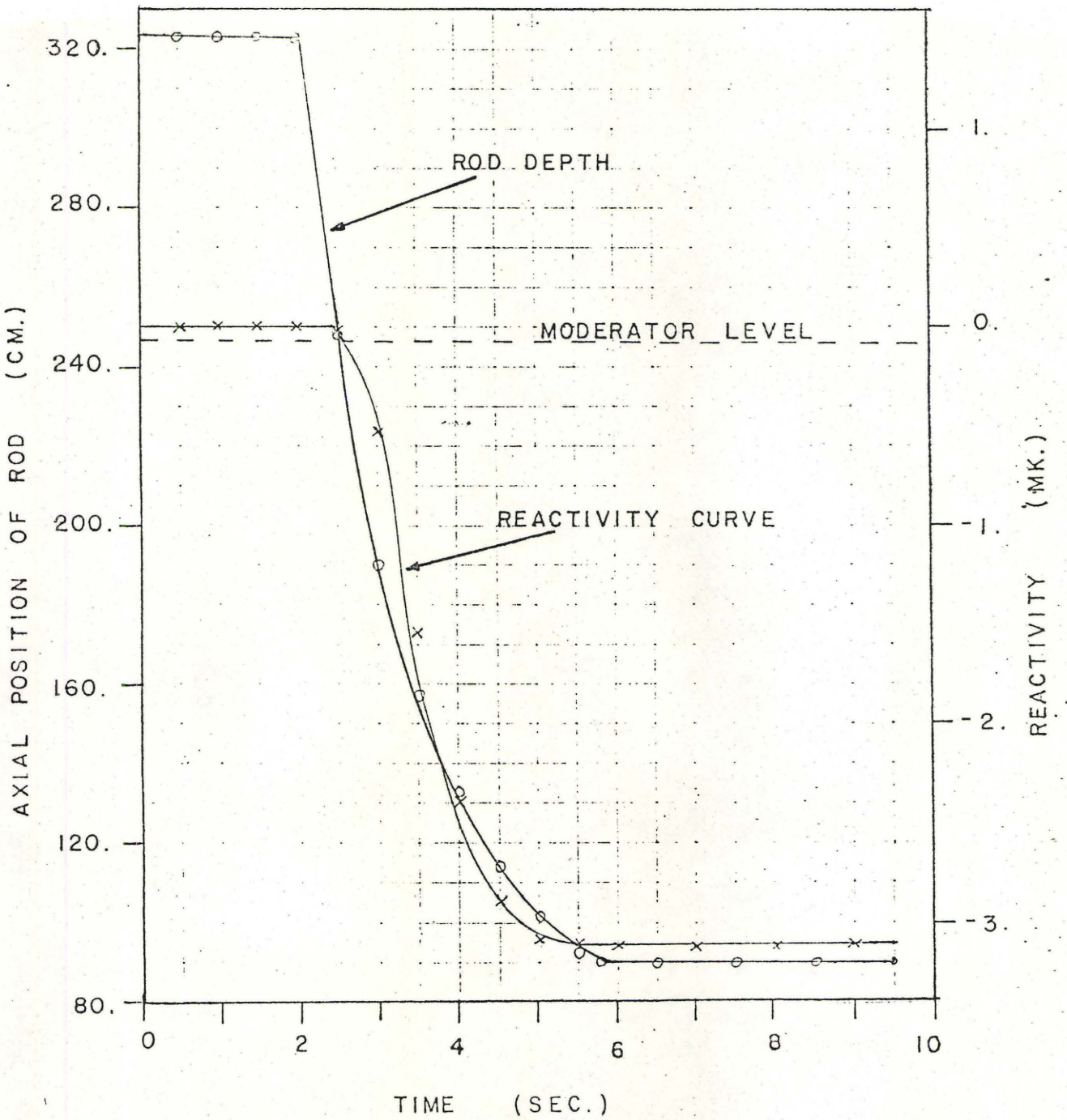

FIG. 6: ROD DEPTH VERSUS TIME DURING THE ROD DROP AND THE CORRESPONDING REACTIVITY CHANGE

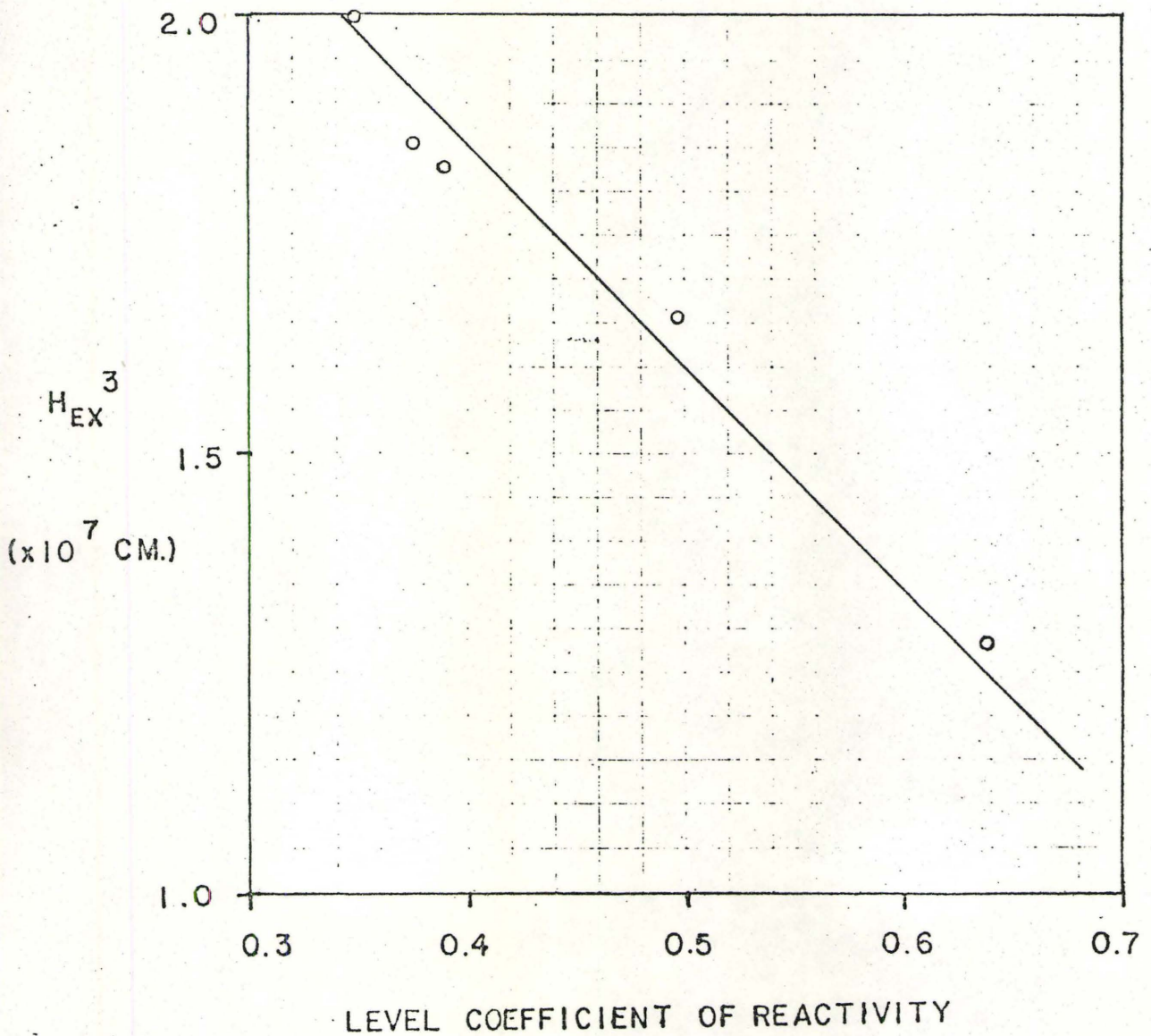

FIG. 7: THE PLOG OF H_{EX}^3 VS. LCR USED TO OBTAIN EQ. (4).

(a)

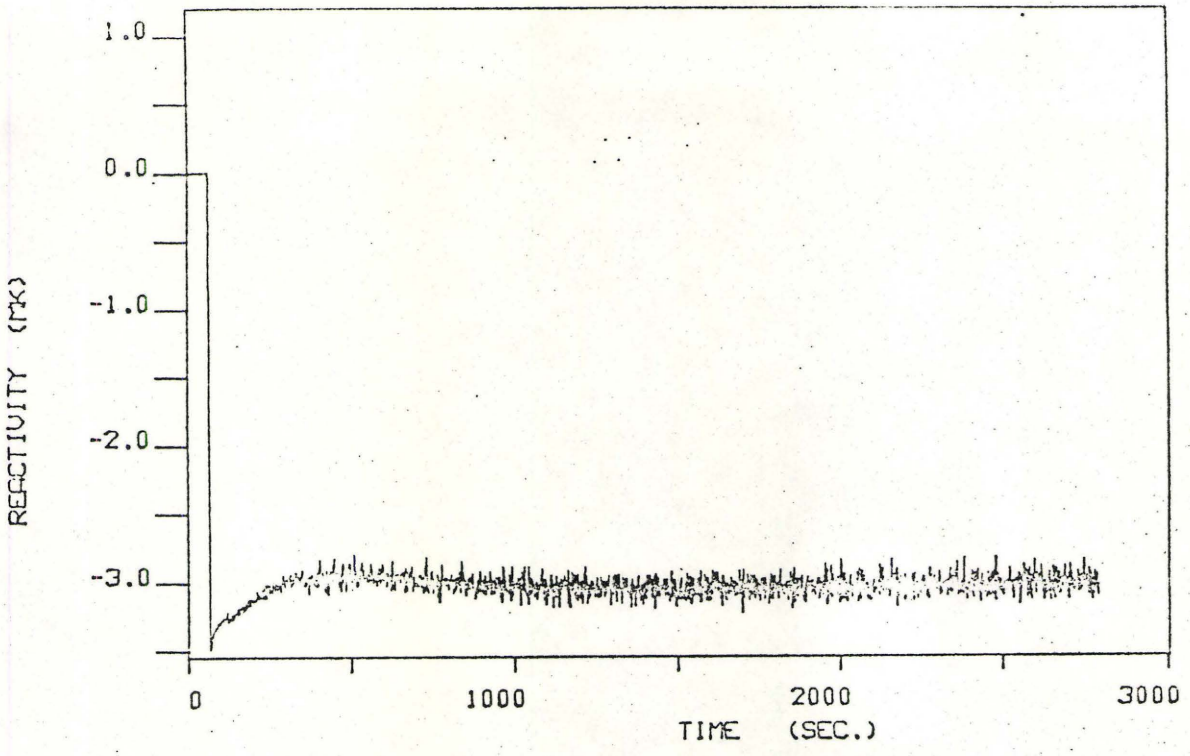

(b)

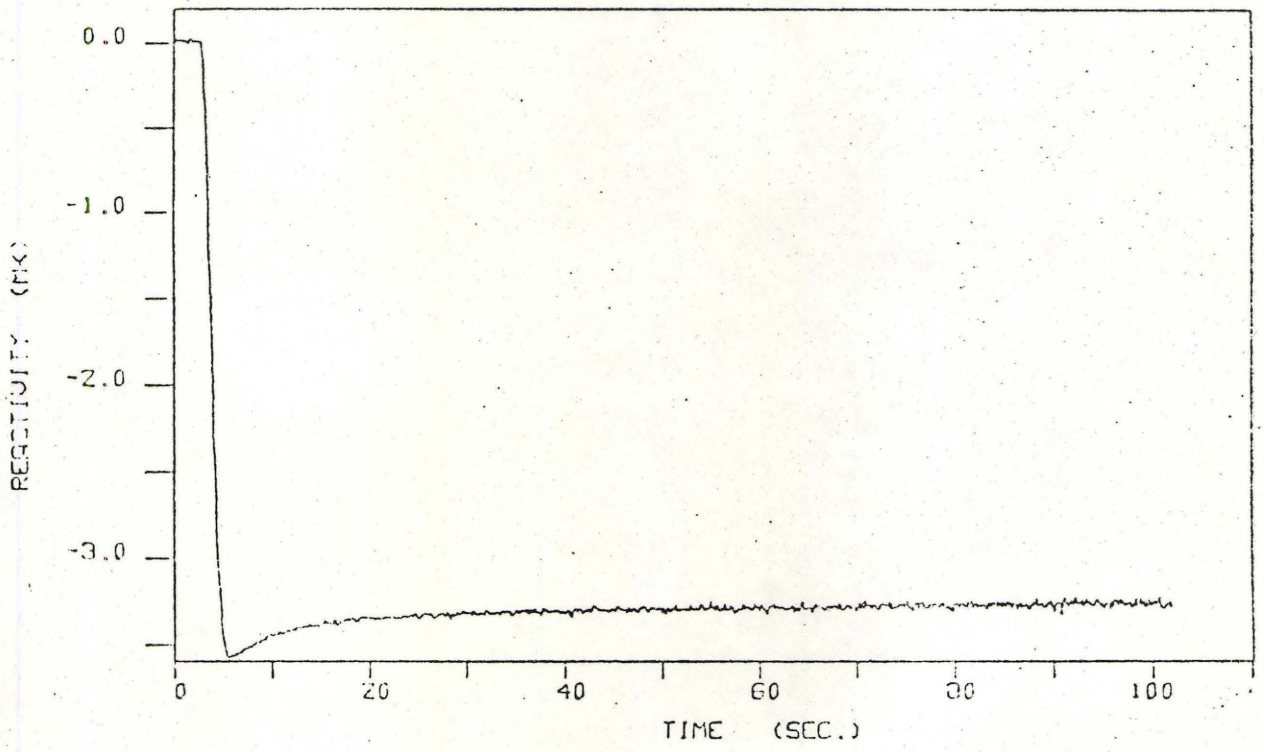

FIG. 8: REACTIVITY vs. TIME AT DETECTOR POSITIONS L1E (A) AND J1E (B) WITH SHUTOFF ROD AT CENTRE.

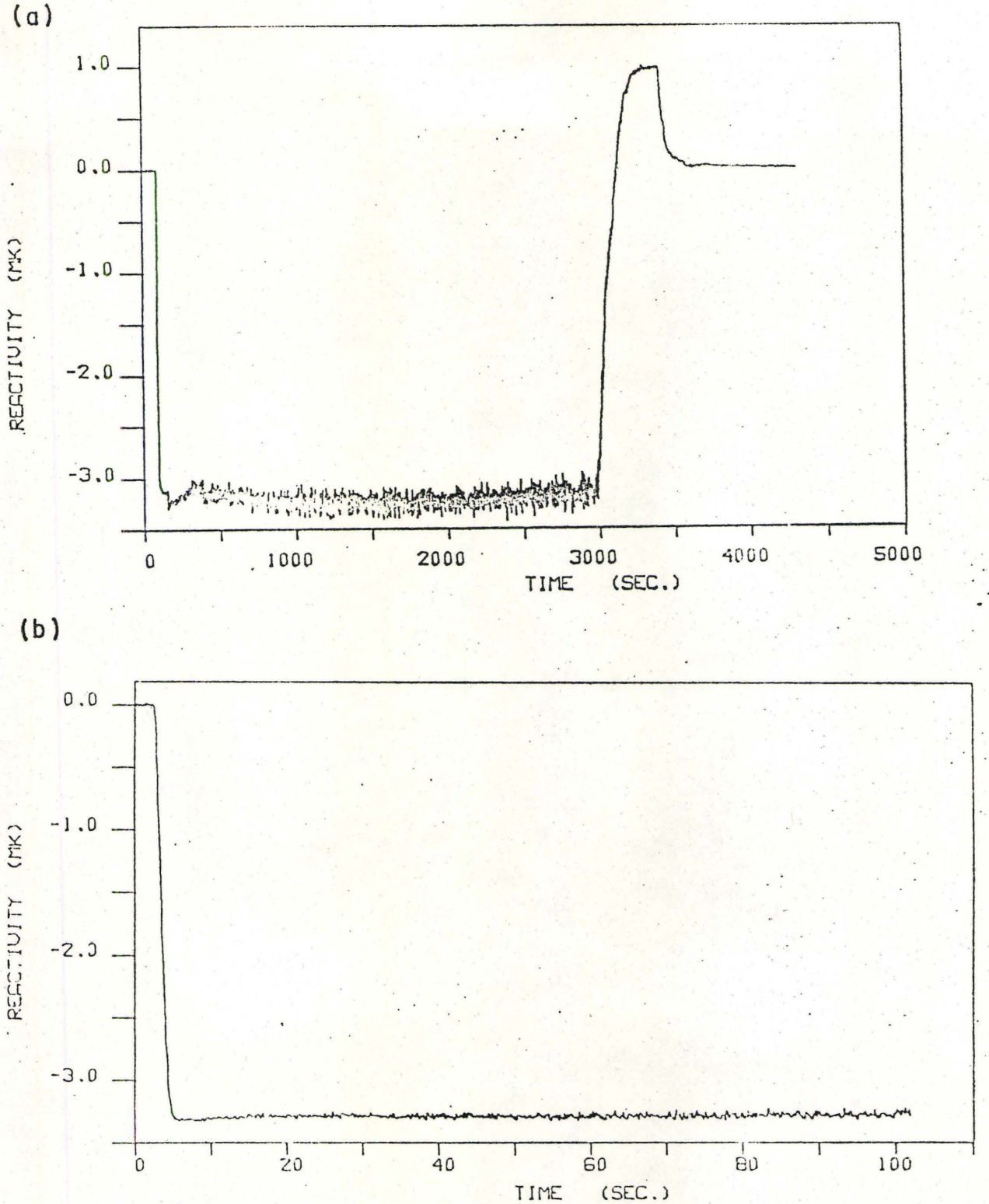

FIG. 9: REACTIVITY vs. TIME AT DETECTOR POSITIONS M1E (A) AND I1E (B) WITH SHUTOFF ROD AT CENTRE.

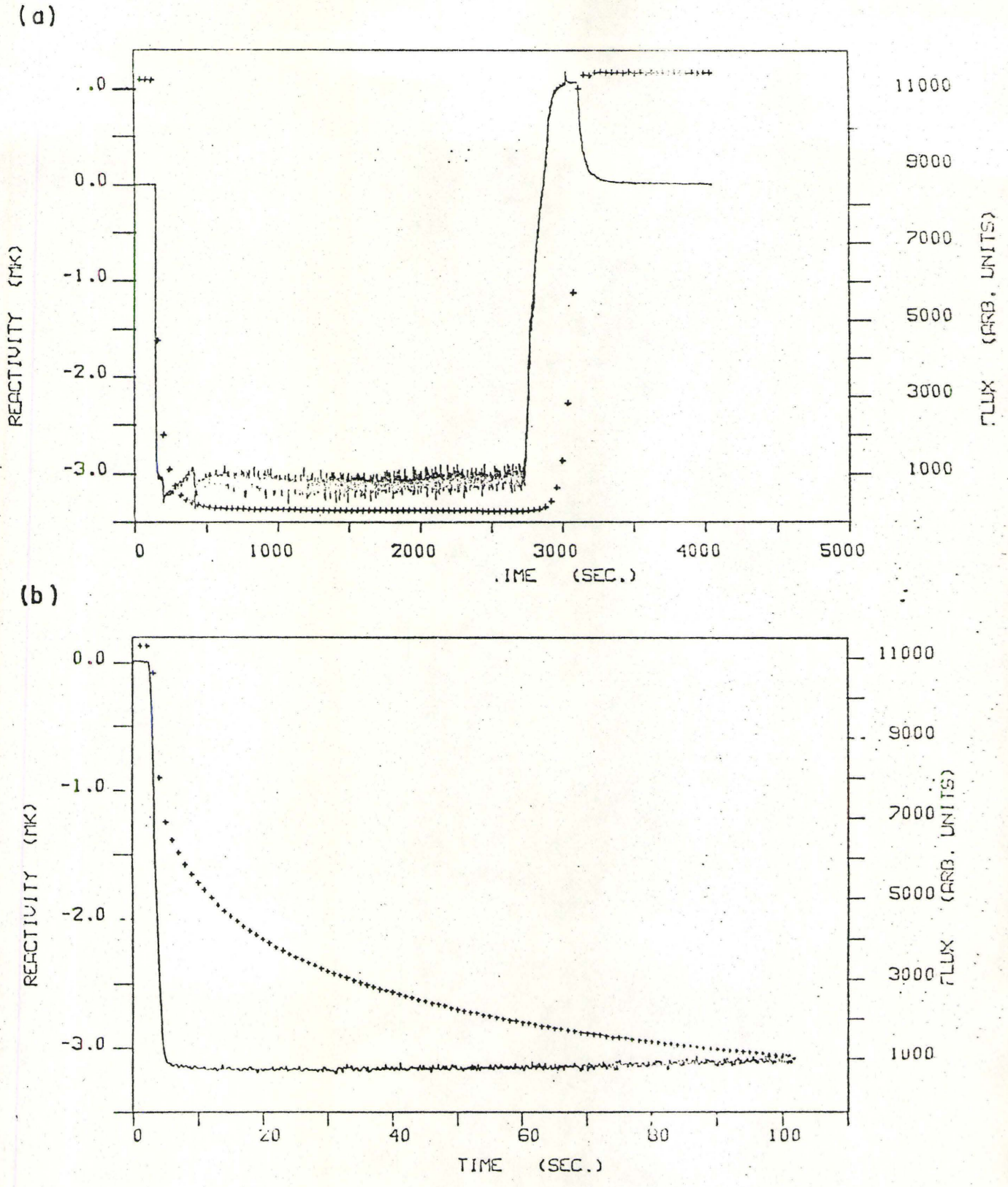

FIG. 10: NEUTRON FLUX AND REACTIVITY vs. TIME AT DETECTOR POSITIONS N1E (A) AND H1E (B) WITH SHUTOFF ROD AT CENTRE.

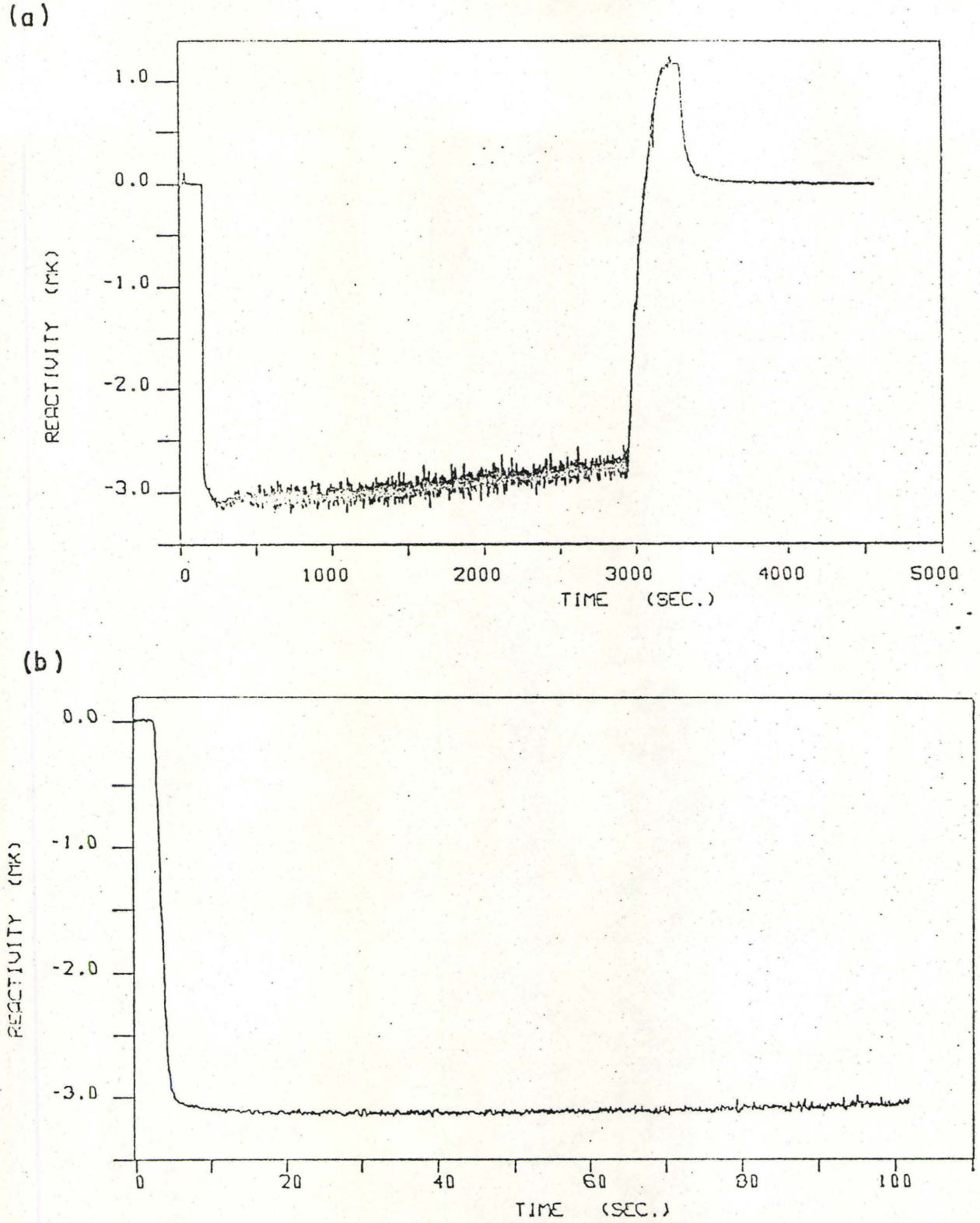

FIG. 11: REACTIVITY vs. TIME AT DETECTOR POSITIONS 01E (A) AND G1E (B) WITH SHUTOFF ROD AT CENTRE

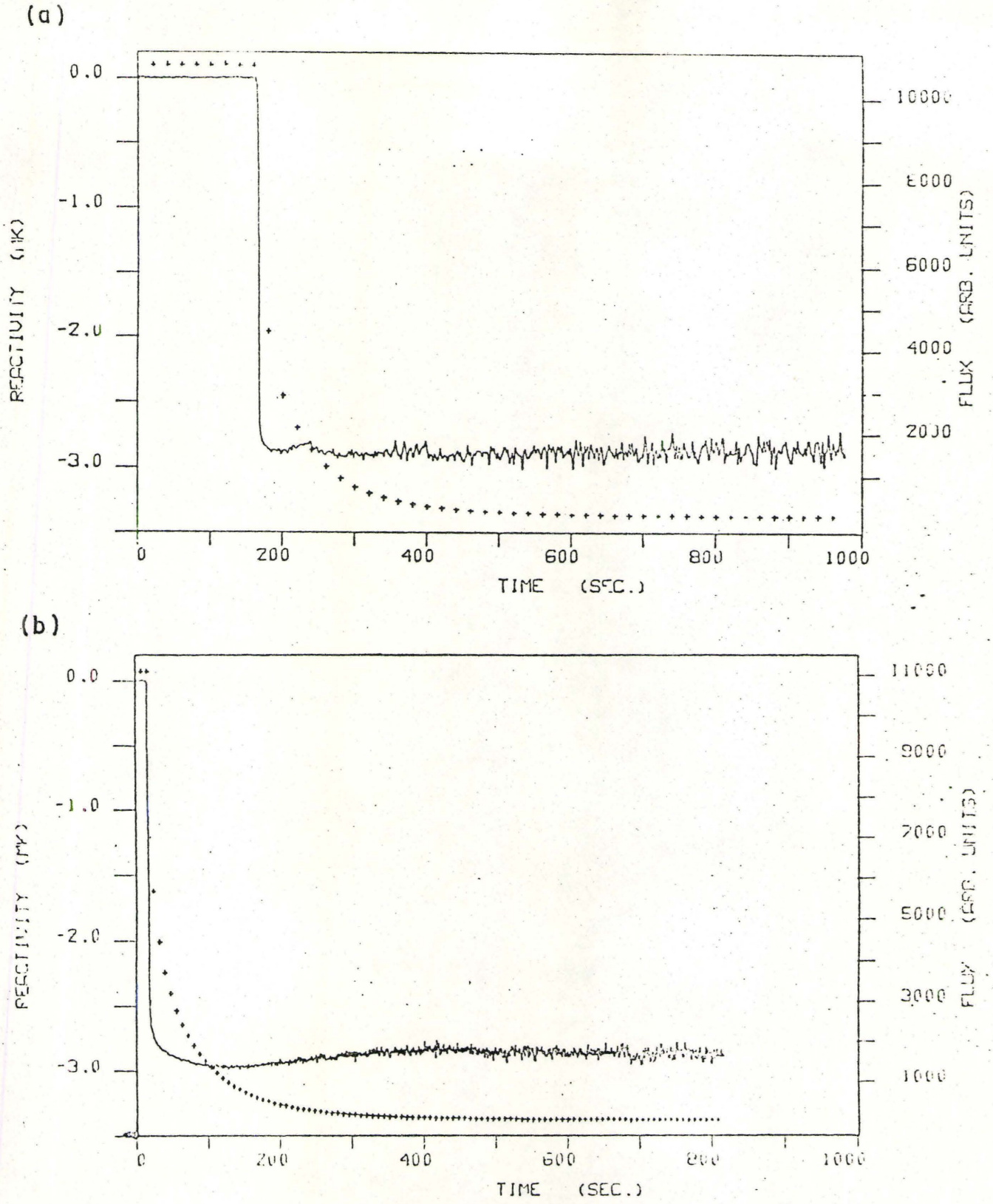

FIG. 12: NEUTRON FLUX AND REACTIVITY vs. TIME AT DETECTOR POSITIONS O1E (A) AND G1E (B) WITH SHUTOFF ROD AT L1W.

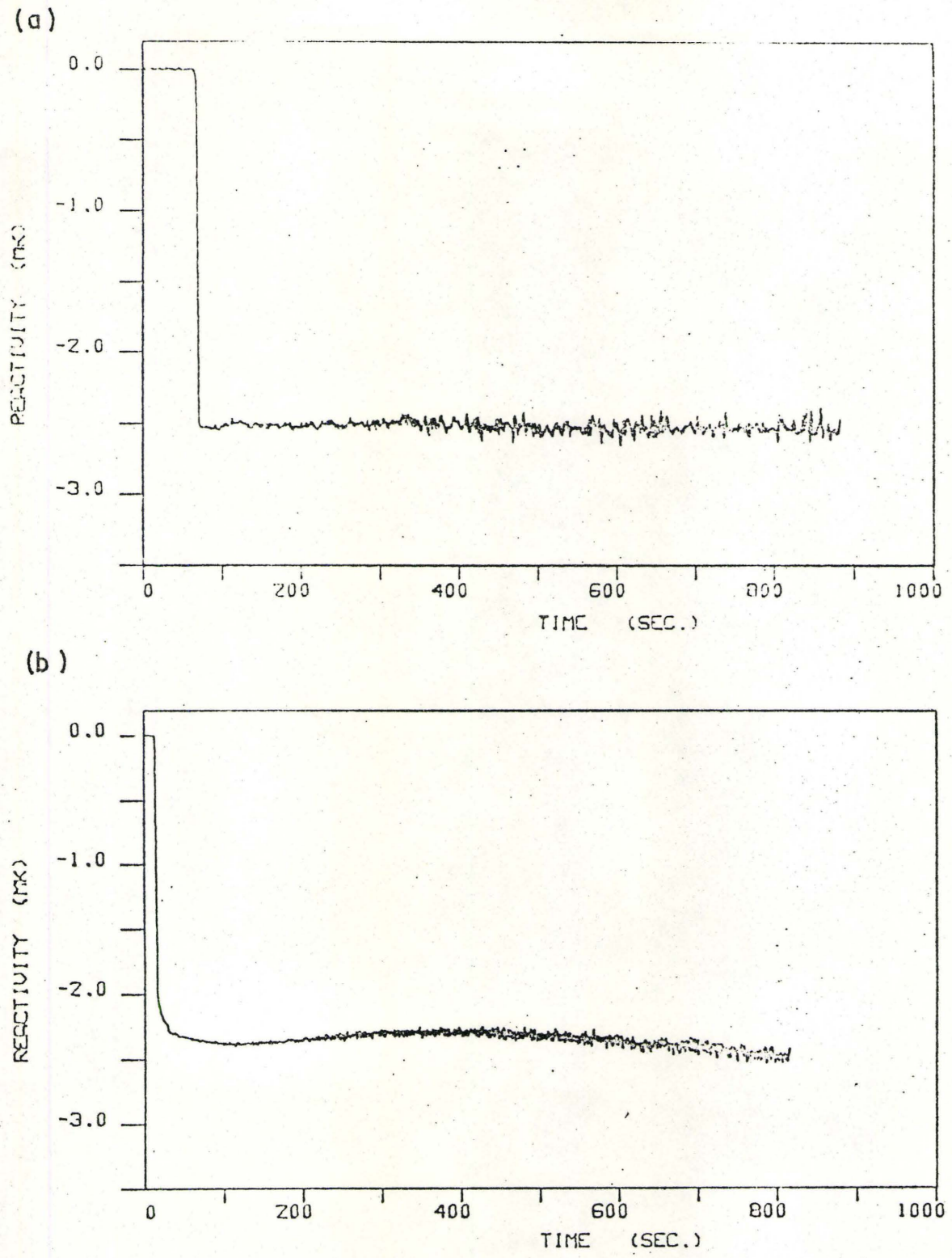

FIG. 13: REACTIVITY vs. TIME AT O1E (A) AND G1E (B) WITH SHUTOFF ROD AT M1W.

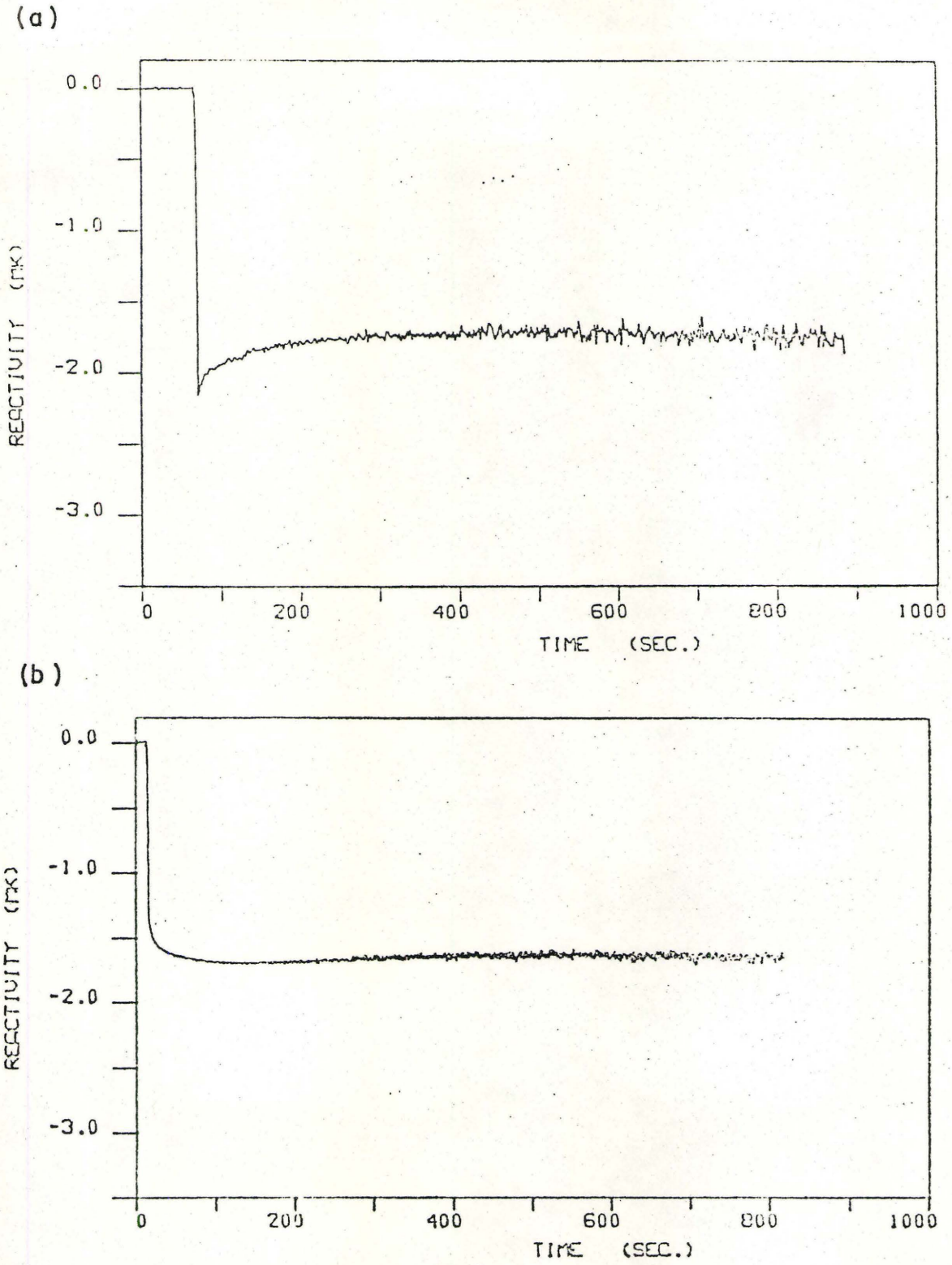

FIG. 14: REACTIVITY vs. TIME AT O1E (A) AND G1E (B) WITH SHUTOFF ROD AT N1W.

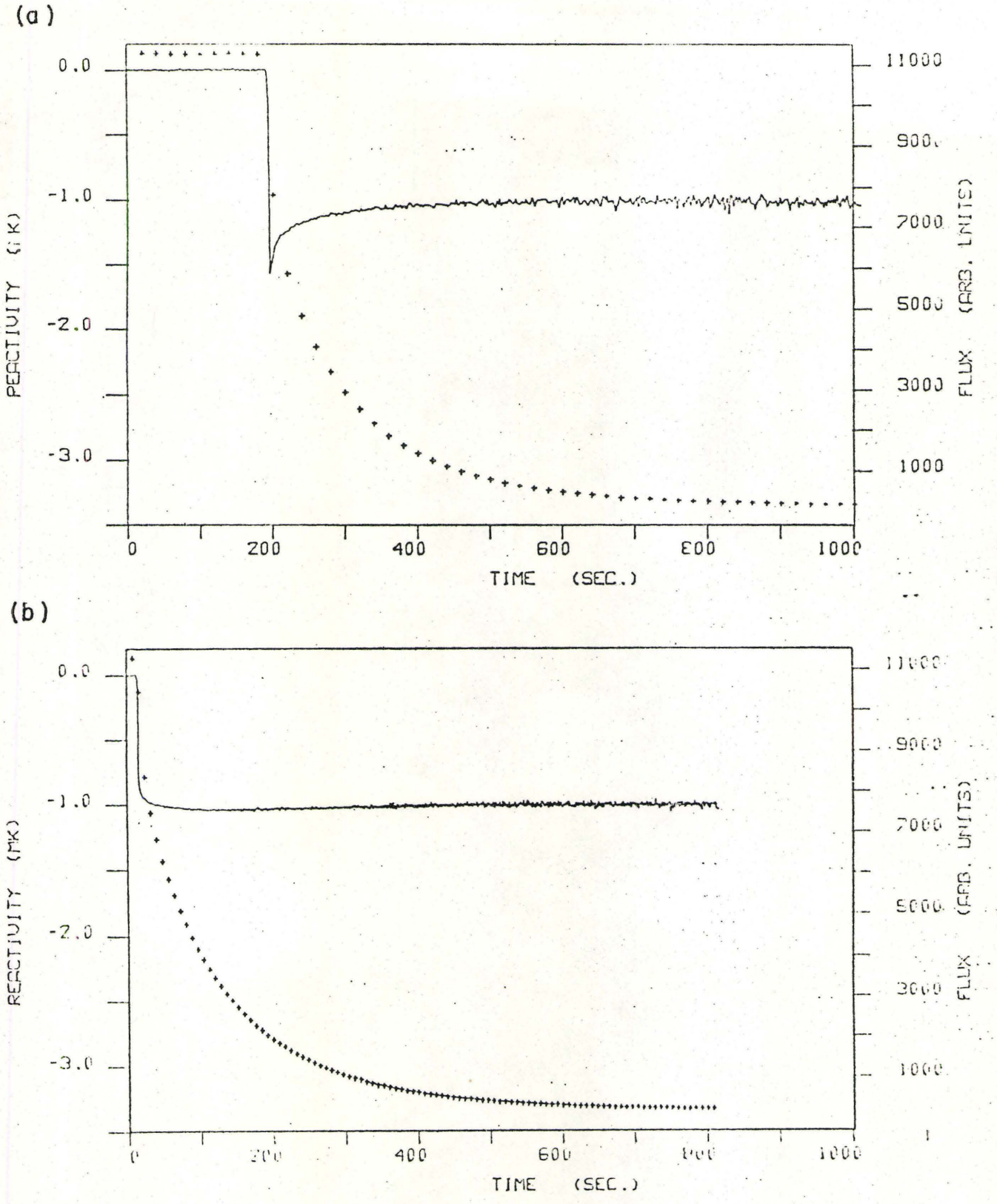

FIG. 15: NEUTRON FLUX AND REACTIVITY vs. TIME AT 01E (A) AND G1E (B) WITH SHUTOFF ROD AT 01W.

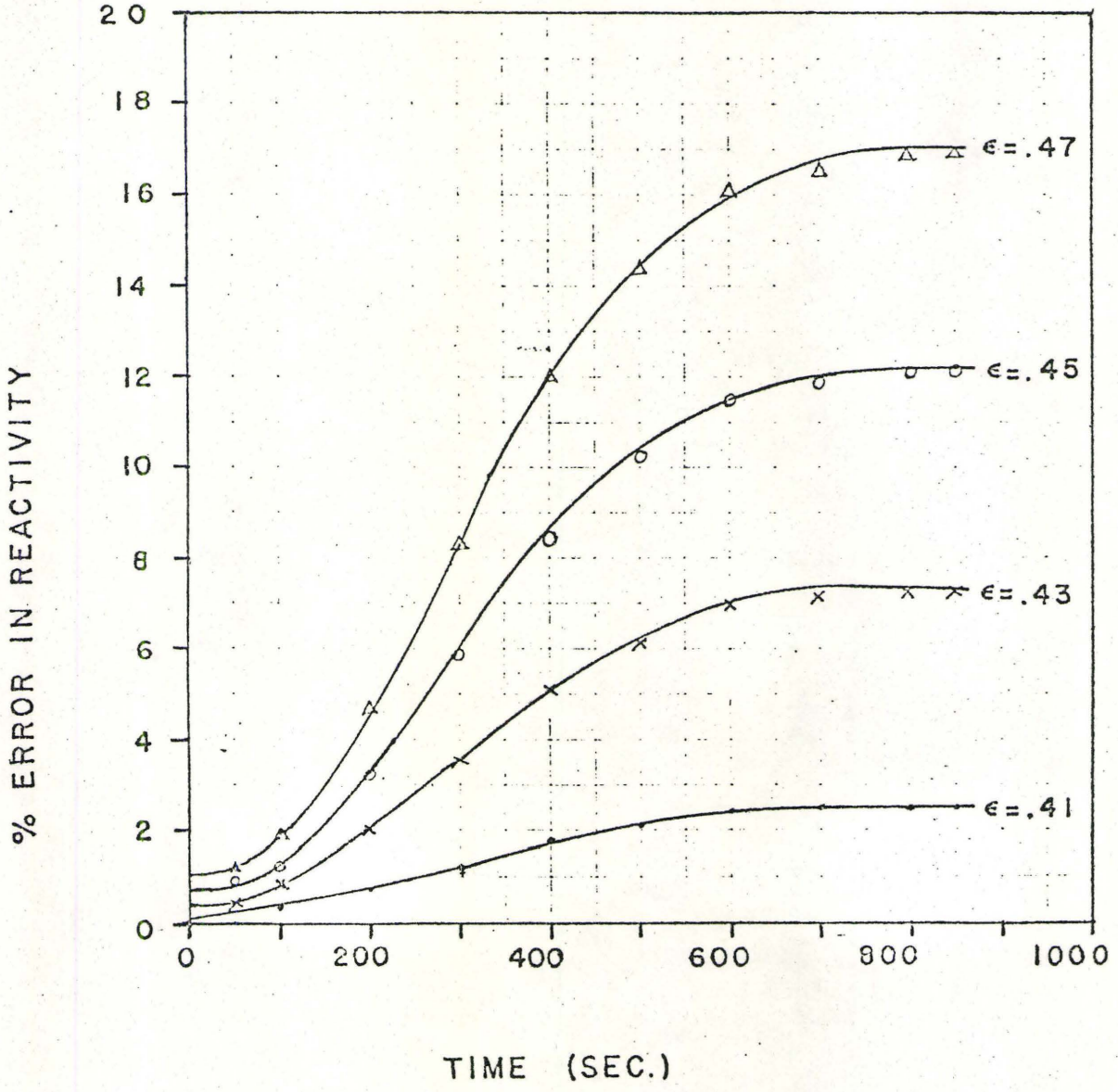

FIG. 16: THE CHANGE IN ERROR WITH TIME CAUSED BY OVER-ESTIMATING ϵ.

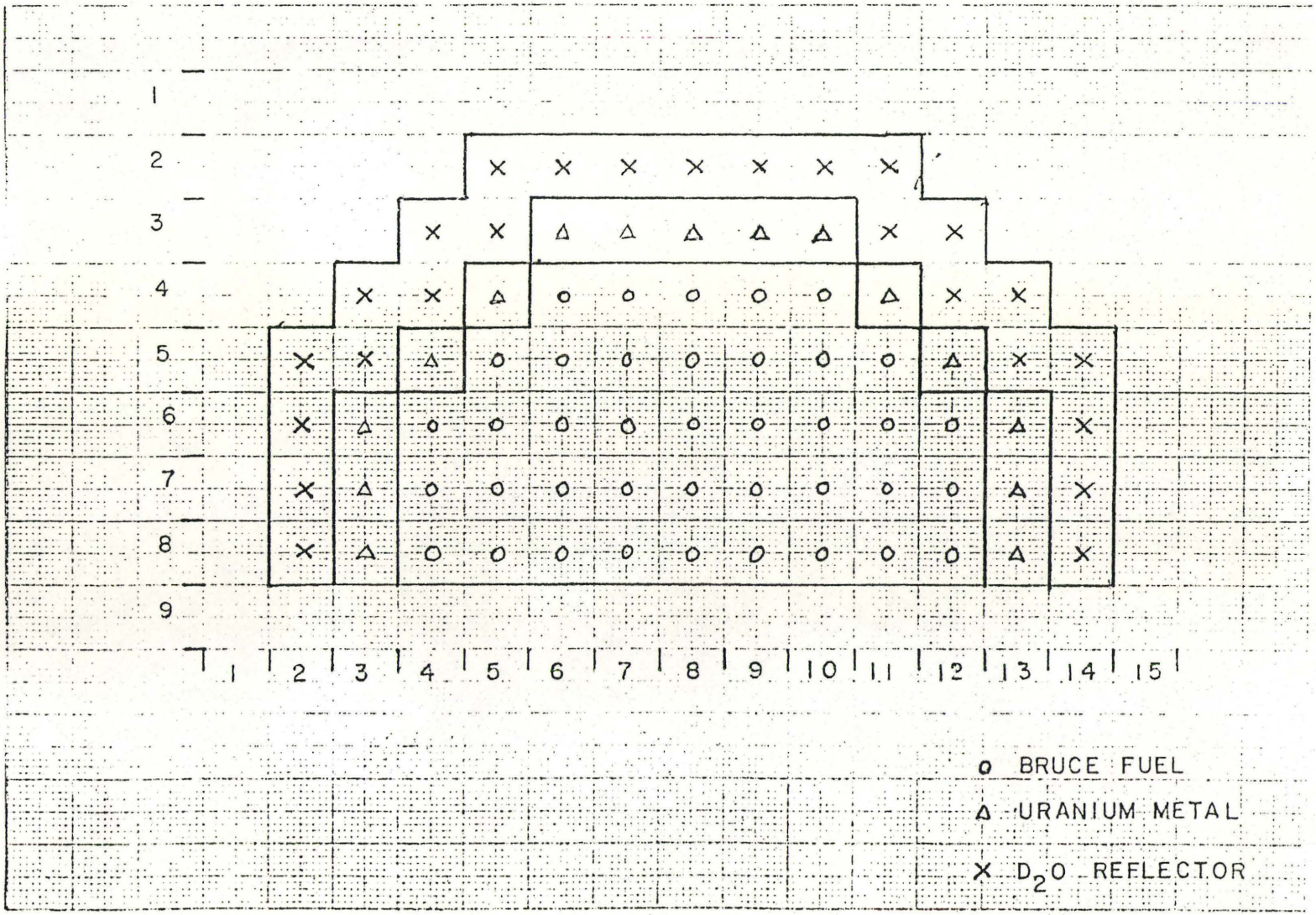

FIG. 17: THE MOCK-UP OF ZED-2 USED IN CERBERUS.

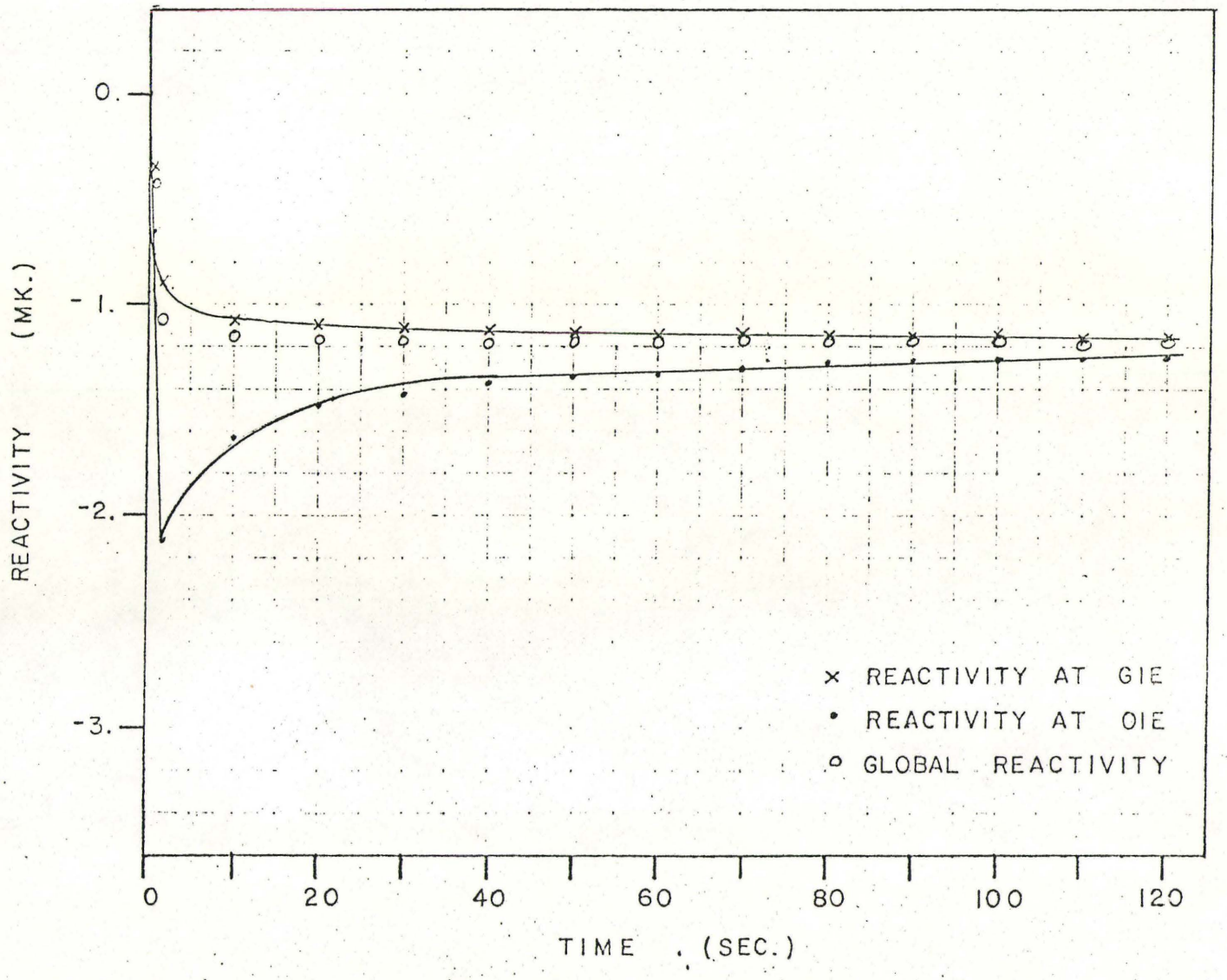

FIG. 18: REACTIVITY VERSUS TIME FOR THE ROD-DROP AT 01W AS DETERMINED BY CERBERUS.

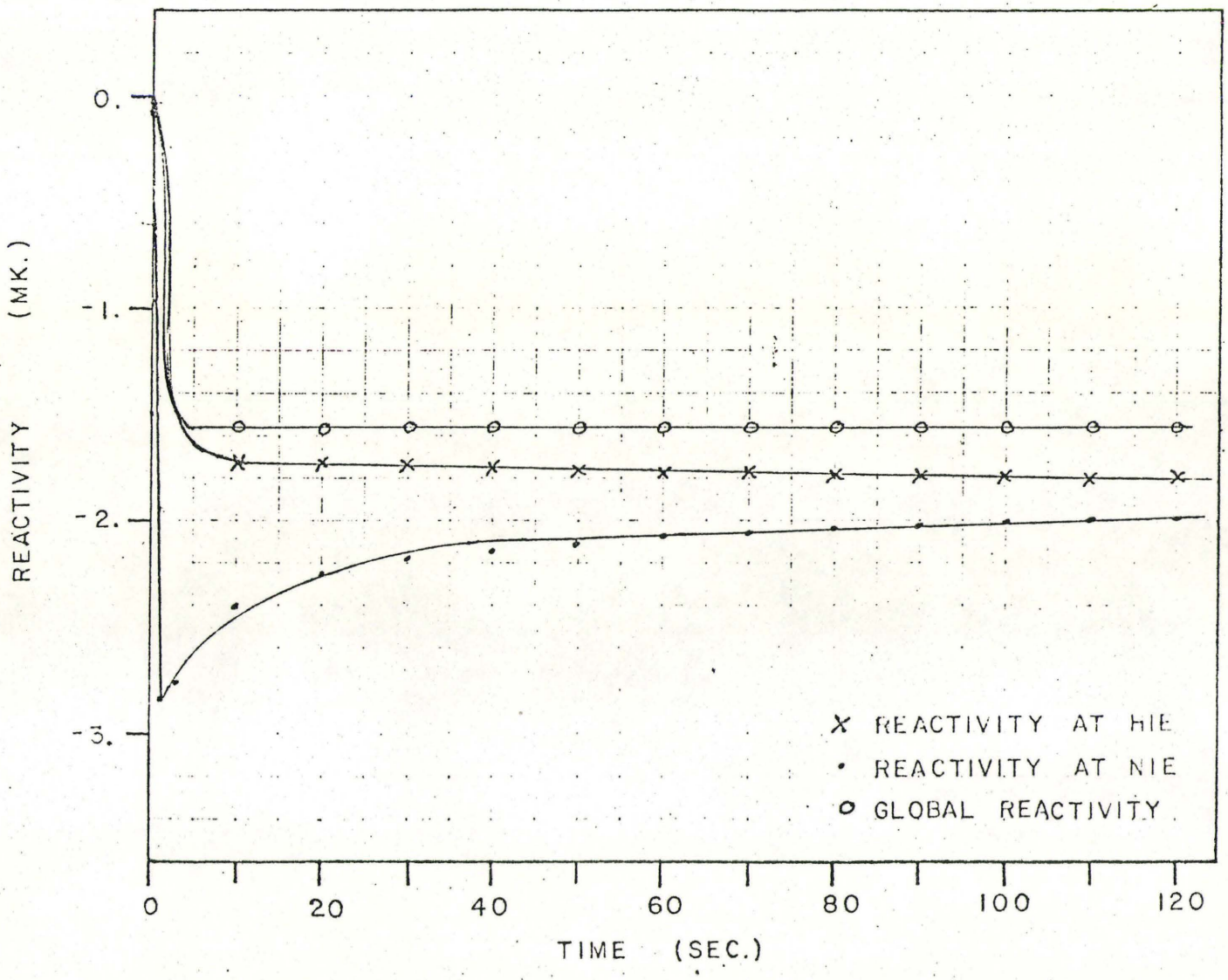

FIG. 19: REACTIVITY vs. TIME FOR THE ROD-DROP AT N1W AS DETERMINED BY CERBERUS.

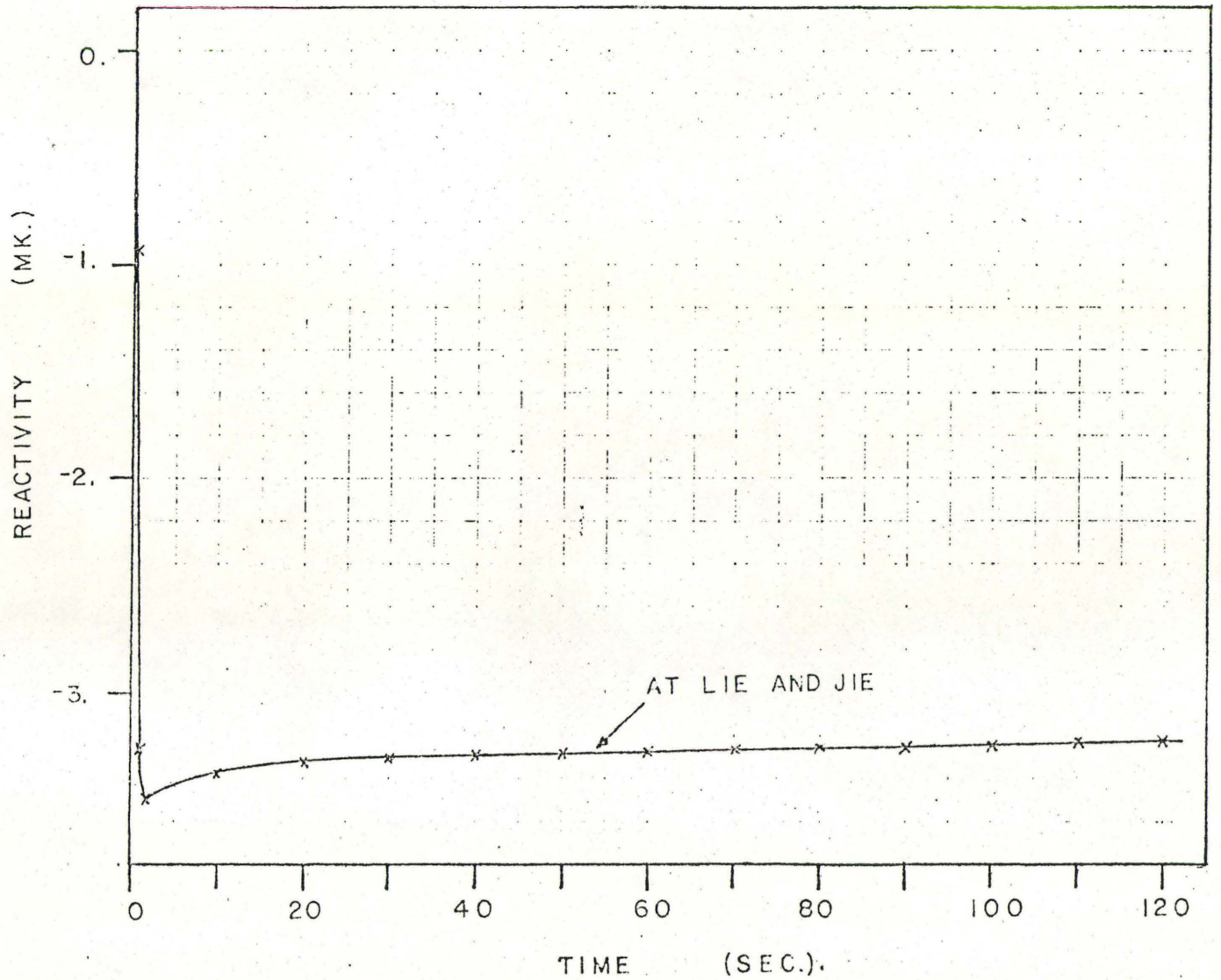

FIG. 20: REACTIVITY VS. TIME FOR THE ROD-DROP AT CENTRE CORE AS DETERMINED BY CERBERUS.

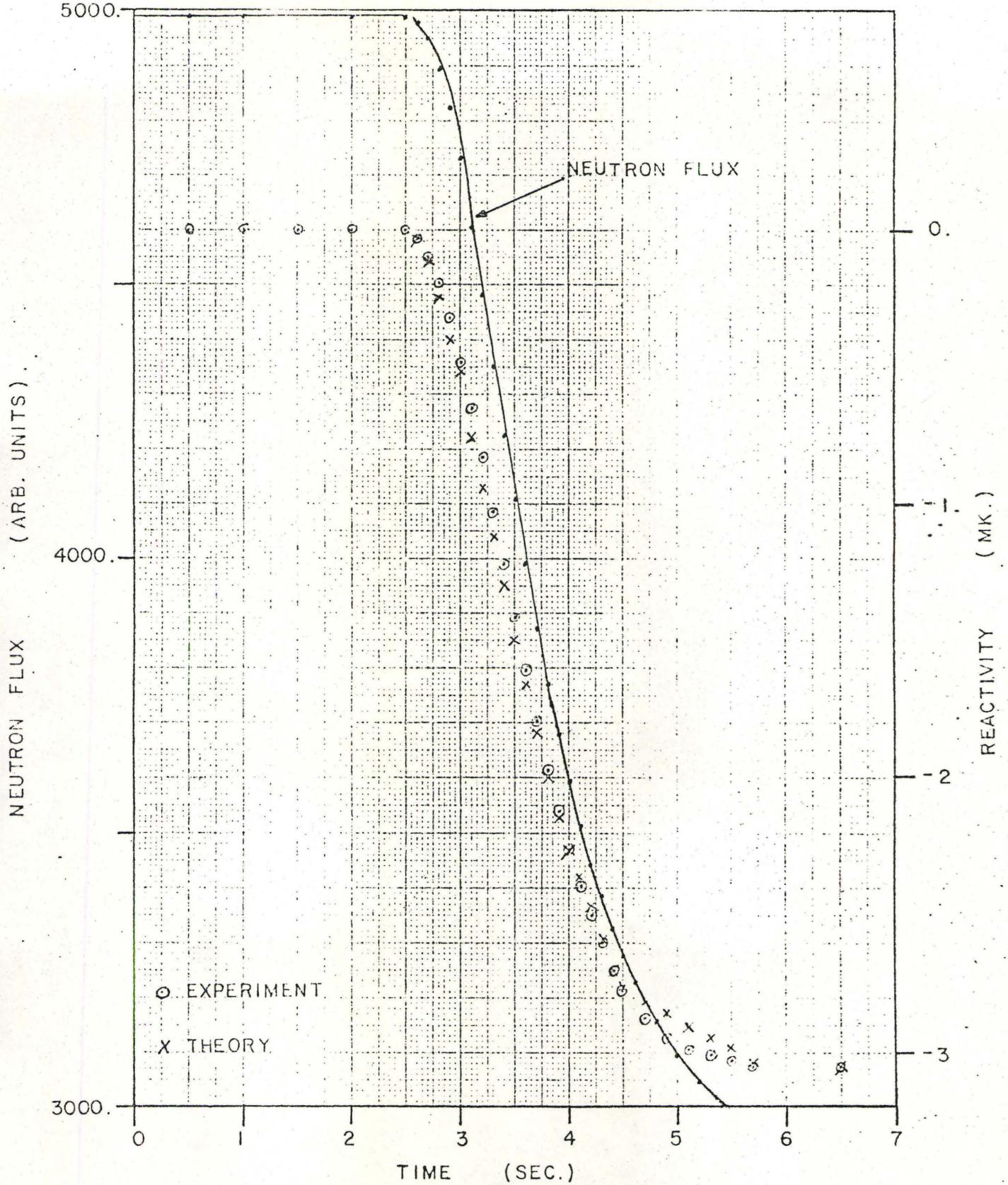

FIG. 21: THE CHANGE IN NEUTRON FLUX DURING THE ROD-DROP AND A COMPARISON OF THE CORRESPONDING REACTIVITY CHANGES OBTAINED FROM EXPERIMENT AND FROM CERBERUS.